Chemical Science

ROYAL SOCIETY OF CHEMISTRY

EDGE ARTICLE

View Article Online
View Journal | View Issue

Cite this: *Chem. Sci.*, 2026, **17**, 3103

All publication charges for this article have been paid for by the Royal Society of Chemistry

Received 12th September 2025
Accepted 5th December 2025

DOI: 10.1039/d5sc07027a

rsc.li/chemical-science

Lipid-regulated assembly mechanisms and functional energetics of the essential bacterial chaperone BamA

Anjana George, Anusree Mulanthala Raj, Akanksha Gajanan Patil, Varsha Kumari and Radhakrishnan Mahalakshmi *

BamA is a highly conserved essential outer membrane chaperone of all Gram-negative bacteria. Our understanding of the BamA machinery remains incomplete, delaying knowledge-based antibacterial design. Here, we report the first detailed identification of molecular elements indispensable for BamA folding, stability, and function. BamA displays two unique transition state structures and folding pathways in phosphatidylethanolamine (PE)- and phosphatidylglycerol (PG)-containing membranes. PE retards BamA folding; once folded, PE lowers stability of the N-terminal β-strands. In interesting contrast, PG promotes directional folding of BamA, and rigidifies the protein structure by lowering its conformational sampling space. We demonstrate that BamA β5–L4–β8 is an obligatory late-assembly zone in both PE and PG. Thermodynamic free energy measurements show BamA as membrane-anchored at β11–β15 and destabilized at β2–β7 for its N-terminal gating function, with a C-terminal structural kink at β16. We show how BamA function links directly with (i) structures of PE-specific transition states, and (ii) zonal (de)stabilization hotspots at β5–L4–β8, β9–L5–β10, and β16-K^{808}. We propose that these sites can now serve as novel hotspots for structure-based design of peptidomimetics to target multi-drug resistant Gram-negative pathogens.

Introduction

The global threat posed by the alarming increase in fatalities from antimicrobial resistance, particularly from ESKAPEE (*Enterococcus faecium*, *Staphylococcus aureus*, *Klebsiella pneumoniae*, *Acinetobacter baumannii*, *Pseudomonas aeruginosa*, *Enterobacter* species, and *Escherichia coli*)[1] pathogens, demands immediate interventions with novel synergistic peptidotherapeutics that categorically target essential microbial machinery.[2] In Gram-negative bacteria, the outer membrane (OM) is composed of lipopolysaccharides in the outer leaflet, phospholipids in the inner leaflet, and β-barrel outer membrane proteins (OMPs) that together function as the first line of communication between the bacterium and its environment. OMPs execute crucial physiological and structural functions for the bacterium, with OMP modifications causing antimicrobial resistance.[3–8] The correct folding and assembly of most OMPs in the bacterial outer membrane necessitates the β-Barrel Assembly Machinery (BAM),[9] which is made up of the highly conserved membrane protein insertase BamA as its core functional component, and four lipoproteins BamB-E (Fig. 1a). In addition to folding OMPs, BamA is critical for OM integrity and envelope stress response.[10–12] BamA is functionally invariable with a high degree of conservation, and is an essential OMP in Gram-negative bacteria.[13,14] Not surprisingly, BamA mutations cause lethality in Gram-negative bacteria.[15–17] Hence, BamA is one of the few excellent targets for next-generation antimicrobials.[18–22] However, despite several structural,[23–27] biochemical,[28,29] and functional[13,30–34] studies of BamA, we have exceedingly limited understanding of its key molecular regulators.

Escherichia coli BamA ($BamA^{Ec}$) is an 810-residue protein, which is incorporated in the membrane by an existing BAM complex.[31,35] Mature $BamA^{Ec}$ possesses an N-terminal extramembranous (periplasmic) pentameric repeat of the Polypeptide Transport-Associated (POTRA) domain (POTRA1-5), and a C-terminal transmembrane β-barrel domain (TMD). Nascent OMP (nOMP) substrates associated with periplasmic chaperones (*e.g.*, SurA and Skp) are offloaded at the POTRA domains, where they then associate with the TMD of an existing BamA for assembly.[31,35,36] Several mechanisms of BAM-assisted nOMP folding have been proposed.[37] These involve various components of the BAM complex to varying degrees, including the weak H-bonding at the BamA β-barrel seam, TMD luminal residues, TMD-POTRA conformational changes, BamA loop 6 (L6) dynamics, contributions of BamB-E, and BAM-SurA interactions.[24,27,35] The N-terminal strands of folded BamA, which form part of the BAM complex (we refer to this as $BamA^{M}$), can

Molecular Biophysics Laboratory, Department of Biological Sciences, Indian Institute of Science Education and Research, Bhopal – 462066, India. E-mail: maha@iiserb.ac.in; mahas999@gmail.com

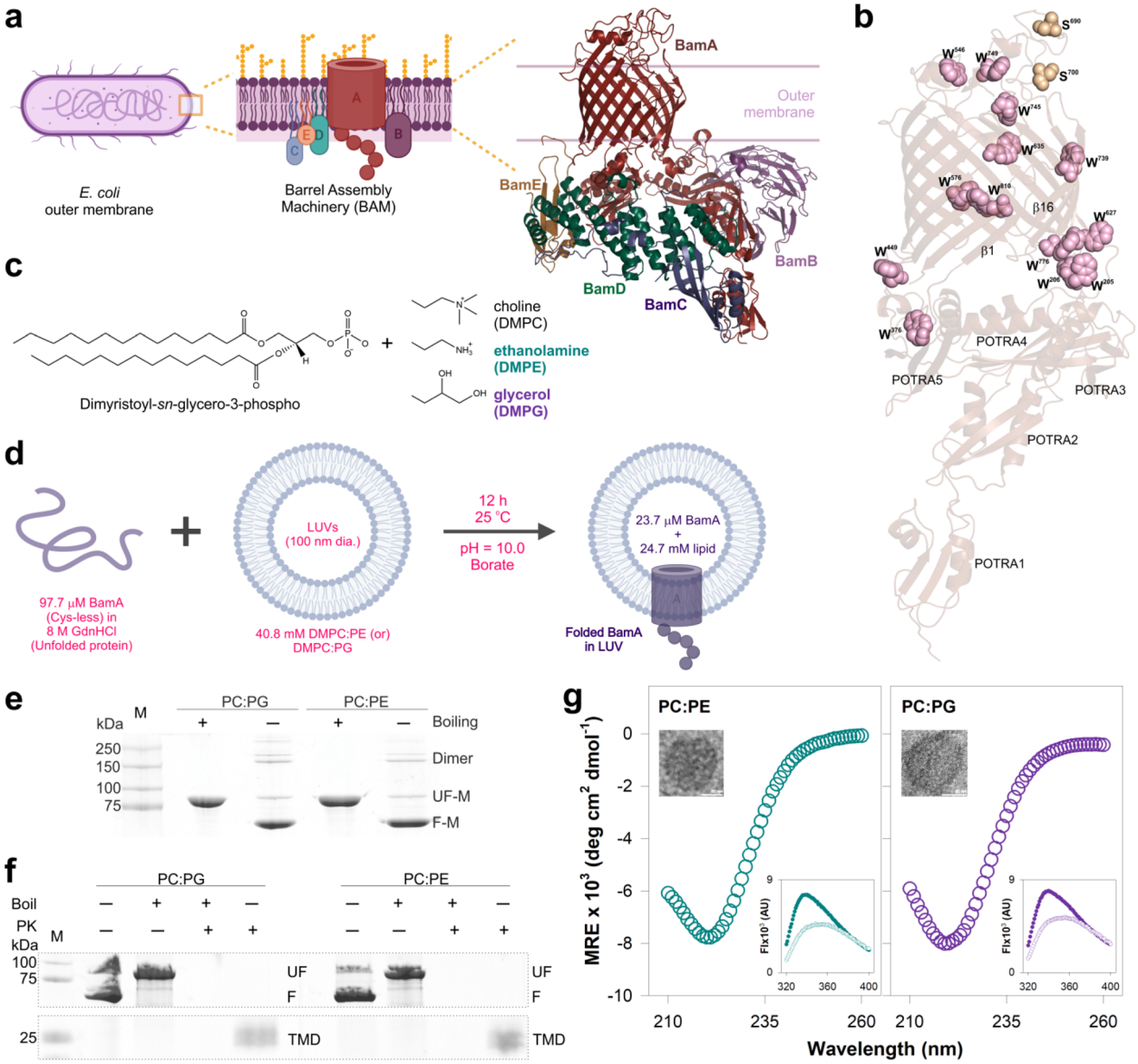

Fig. 1 Assembly of BamA in host–guest membranes and validation of folding. (a) Cartoon representation of a typical *E. coli* cell (left), illustrating the BAM complex in its OM (middle). BAM facilitates energy-independent insertion of nOMPs. BamA, with its N-terminal POTRA domain and C-terminal 16-stranded transmembrane β-barrel (left), along with the four lipoproteins BamB-E, together constitute the BAM complex. Created using Biorender.com and PyMOL. (b) The 13 Trp residues of BamA (PDB ID: 5AYW) are highlighted on the protein structure. Also indicated are the positions of the two Cys → Ser substitutions on loop 6 we carried out to obtain Cys-less BamA. (c) Chemical structures of the 14-C lipids used in this study. (d) BamA folding in LUV membranes (borate buffer, pH 10.0) by rapid dilution of the unfolded protein to achieve an LPR of 1042:1 results in unidirectional BamA assembly (schematic created using Biorender.com) (also see Table S1). (e) Folded BamA displays an electrophoretic mobility shift distinct from the unfolded protein in cold Tricine-SDS-PAGE, and (f) resistance to pulse proteolysis by proteinase K (PK), in both PE- and PG-containing membranes (also see Fig. S3 and S4). As seen with other bacterial OMPs,[51,77] BamA exhibits faster electrophoretic mobility upon folding. The membrane protects the β-barrel from proteolysis, while the N-terminal extramembranous POTRA domain, albeit folded, undergoes near-complete proteolytic digestion.[48] The latter observation confirms a unidirectional insertion of BamA in the vesicle, with the extramembranous loops positioned within the vesicle lumen and the water-soluble POTRA oriented outside the vesicle (as illustrated in 1d). (g) Folded BamA displays a far-UV circular dichroism spectrum characteristic of a β-rich protein upon folding in both PC:PE (left, teal) and PC:PG (right, purple) membranes, with molar ellipticity (ME) values of -6.26×10^6 deg cm^2 dmol^{-1} (PC:PE) and -6.50×10^6 deg cm^2 dmol^{-1} (PC:PG) at 220 nm. TEM images of the LUVs are shown as an inset (top left). An increase in Trp fluorescence emission, accompanied by a blue-shifted $\lambda_{em\text{-}max}$ is also observed upon BamA folding (inset, bottom right; folded: filled circles, unfolded: open circles).

also interconvert between "inward-open" and "laterally-open" states, with its first β-strand (β1) forming transient H-bonds with the C-terminal β-strand of an incoming nOMP in its "laterally-open" state.[31,32]

Despite BAM structures being available from several bacteria, identifying key factors that regulate BamA remains incomplete. This includes (i) the precise folding mechanism of BamA itself, (ii) stability and structural modulators of BamA,

and (iii) the role of the membrane in regulating BamA physicochemical, structural, and functional characteristics. Antimicrobials discovered thus far, which can target structural dynamics and functional features of BamA to varying extents, include darobactin, dynobactin, MRL-494, BamA targeting peptides, and chimeric peptidomimetics.[18,21,26,37–45] These discoveries warrant investigating 'hotspots' in BamA that could lead to development of more efficient BamA inhibitors for ESKAPEE pathogens.

Christian B. Anfinsen first proposed that the protein sequence can fold into its correct structure without chaperone assistance.[46] While BamA utilizes BAM-assistance to fold in the cell, we show here that BamA can fold correctly in membrane vesicles independent of its lipoproteins or a pre-existing BAM complex. By characterizing 88 Xaa → Ala BamA mutants, we successfully identified two lipid-specific structures formed transiently during BamA folding, and mapped thermodynamic regulators of the folded BamA β-barrel. We show that BamA folding is stepwise, involves pre-assembly of strands β11–β16 in both phosphatidylethanolamine (PE) and phosphatidylglycerol (PG), and is directional (C → N, β16 → β1) in PG. Once folded, C-terminal residues anchor BamA to the membrane; here, PG enhances BamA stability, and PE augments its function. Folded BamA also displays high kinetic stability, with loop 4 (L4) and BamA-PG interactions serving as structural and functional hotspots. By combining our findings with known features of the BamA structure, we anticipate that structure-based inhibitors designed to target β5–L4–β8, β9–L5–β10 and β16-K^{808} can serve as highly effective checkpoints for the growing antimicrobial resistance.

Results

BamA assembles directionally in PE and PG host–guest membranes

In $BamA^{Ec}$, residues 21–423 constitute the POTRA, and 424–810 form the functionally critical 16-stranded β-barrel that bears 10 of the 13 tryptophans (Fig. 1b). BamA folding efficiency is higher in thinner phosphocholine bilayers,[16,17,47–49] whereas the two non-bilayer forming lipids of the *E. coli* outer membrane, PE (zwitterionic headgroup) and PG (negatively charged headgroup),[50] may inhibit BamA folding (details in SI notes),[13,51,52] and regulate BamA. To identify conditions most conducive to thermodynamic studies of BamA, we extensively screened for membrane lipids, lipid:protein ratios, buffers and temperatures that supported BamA folding by following the change in Trp fluorescence (Table S1, Fig. S1 and S2; details in SI Methods). We additionally generated Cys-less BamA (C^{690} → S, C^{700} → S on L6) to prevent non-specific disulfide bond formation under alkaline conditions. Our screens identified large unilamellar vesicles (LUVs) of 14-C DMPC as sufficient to support reversibility in BamA folding under alkaline conditions (longer chains and unsaturation introduced hysteresis). Doping with either PE or PG supported folding, whereas hysteresis was prominent when both lipids were doped together. Finally, we identified that host–guest LUVs comprising 95% DMPC and 5% DMPE (PC:PE) or 5% DMPG (PC:PG) at a lipid : protein ratio of ∼1000 : 1 and experimental pH = 10.0 supported path-independent folding with an efficiency of ∼100% (Table S1).

We confirmed folding and unidirectional insertion of BamA in both PC:PE and PC:PG LUVs, using electrophoretic mobility shift assays (cold Tricine-SDS-PAGE) (Fig. 1e and S3) and resistance of the C-terminal bilayer-embedded β-barrel to proteolysis (Fig. 1f, S3 and S4). As seen with tryptic digests,[48] proteinase K-digested folded BamA retains a diffuse band at ∼25–30 kDa corresponding to the TMD. This complete proteolytic processing of the POTRA suggests that BamA inserts directionally into the LUV (POTRA outside and loops positioned in the LUV core; Fig. 1f, S3 and S4). Our measurements of secondary structure content using far-UV circular dichroism spectroscopy provided per-residue ellipticity of $\sim -8.0 \times 10^3$ deg cm^2 dmol^{-1} res^{-1} at 220 nm (Fig. 1g), comparable to previous studies,[48,49] confirming the structuring of BamA in both membranes. BamA also displays a hyperchromic and hypsochromic shift of Trp fluorescence emission when it folds from the polar GdnHCl to the hydrophobic membrane environment (Fig. 1g insets). Fluorescence profiles also confirmed that BamA retained its well-folded state in both membranes for >50 days (Fig. S5); therefore, as seen in other membrane proteins,[53,54] folded BamA possesses high kinetic stability. Overall, BamA assembles directionally, and remains stable and structured, in both PE- and PG-membranes.

Functional significance of lipid-dependent zonal thermodynamic stability of BamA

Next, we measured the thermodynamic stability of BamA, using [GdnHCl] as the chemical denaturant and total Trp fluorescence emission as the reporter (Fig. 1g inset, S1). In both membranes, BamA displays a two-state (un)folding transition (Fig. 2a, S5 and S6), with the measured change in folding free energy $\Delta G_F^{0,H_2O}$ of -13.04 ± 0.34 kcal mol^{-1} in PC:PE and -13.12 ± 0.61 kcal mol^{-1} in PC:PG. This high thermodynamic stability is effected in both membranes by the high cooperativity of folding ($M_{eq,F} = -6.4 \pm 0.11$ kcal mol^{-1} M^{-1} in PC:PE and -6.3 ± 0.18 kcal mol^{-1} M^{-1} in PC:PG), which is higher than projected estimates from 8-stranded β-barrels (*e.g.*, OmpA[55] $\Delta G_F^{0,H_2O} = -3.4$ kcal mol^{-1}, $M_{eq,F} = -1.1$ kcal mol^{-1} M^{-1}). Furthermore, the end-state β-barrel is stabilized by a substantial kinetic contribution that slows BamA unfolding in a lipid-dependent manner (2-fold slower in PG; Fig. 2b and S5).

We reasoned that lipid-facing residues would play a primary role in BamA's end-state stability. Hence, to assess whether BamA thermodynamic characteristics are PE/PG-dependent, we deduced the free energy contribution of each lipid-facing side chain ($\Delta\Delta G_F^{0,H_2O}$), by systematically substituting the 88 lipid-facing TMD residues and generating 88 BamA Xaa→Ala mutant variants (Fig. 2c and S7; SI Methods). In both membranes, each Ala-variant retains the two-state cooperative transition ($M_{eq,F}$) of the parent BamA (Fig. 2d and S7). Mutants also show two-state unfolding transitions, and like wild-type BamA, the unfolding equilibrates slower than the folding (Fig. S8). We classified substitutions with a minimal effect on the measured $\Delta G_F^{0,H_2O}$ as WT-like, and those with $\Delta G_F^{0,H_2O}$ >5%

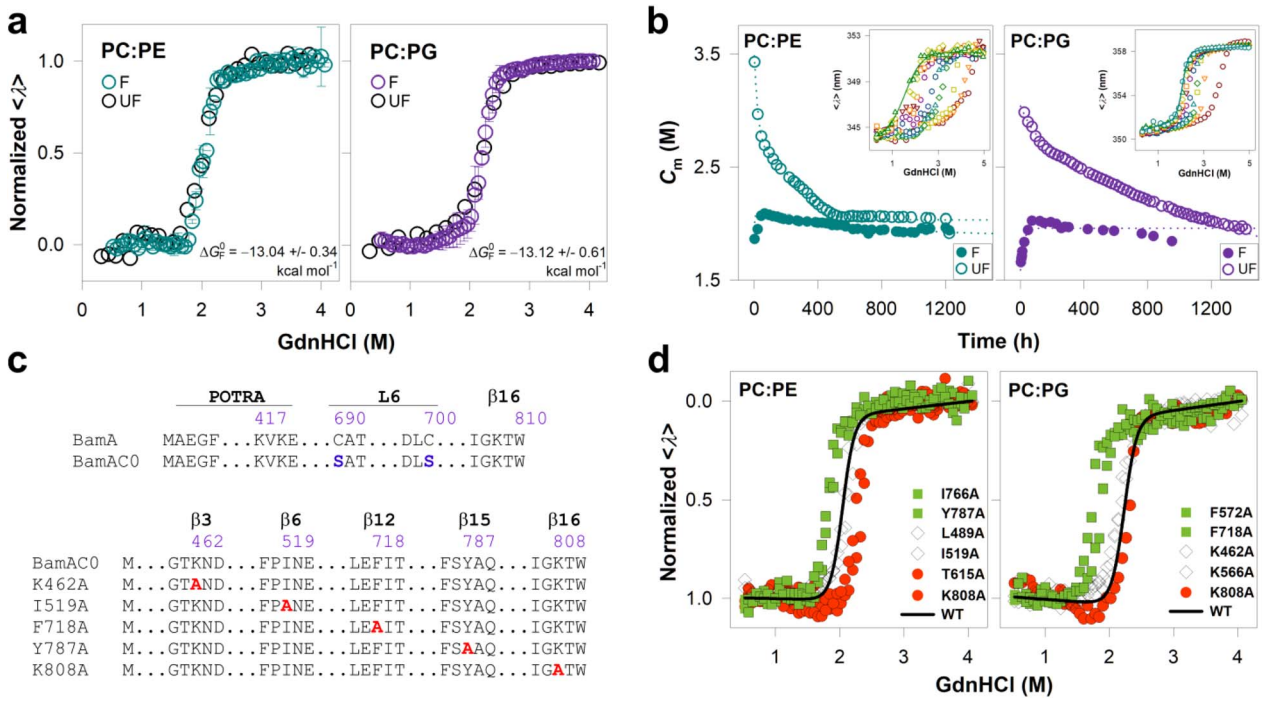

Fig. 2 BamA exhibits two-state cooperative folding in membrane vesicles. (a) End-state equilibrium profiles of BamA monitored using Trp fluorescence in both PC:PE and PC:PG vesicles. The 120-h folding equilibrium profiles are shown with error bars from two independent experiments. Representative unfolding profiles are also superimposed here (PC:PE-500-h; PC:PG-816-h). The mid-point of each transition (C_m) is 2.04 ± 0.05 M (PC:PE) and 2.08 ± 0.10 M (PC:PG). Errors are from five independent experiments. (b) BamA folding equilibrates in 120 h, and unfolding equilibrates in ~20 days in PC:PE and ~34 days in PC:PG. Shown here is the change in C_m with time for one representative folding (filled circles) and unfolding (open circles) titration. Insets: representative unfolding titrations (time course; red → green) (complete data in Fig. S5). BamA folding is a highly cooperative process with a high thermodynamic stability. Yet, BamA unfolding is slower because of the added effect of high kinetic stability. (c) Strategy for the Ala-scanning mutagenesis library of BamA generated in a Cys-less background (top) illustrated using sequences of five representative Ala variants (bottom). The positions of all mutated residues are illustrated in Fig. S7. (d) Representative equilibrium folding profiles of two intrinsically stabilizing (green squares), destabilizing (red circles), and WT-like (white diamonds) residues identified from end-state thermodynamics of BamA Xaa → Ala in both membranes. The fitted line (black) corresponds to WT BamA. Additional data in Fig. S7.

or <5% of BamA as intrinsically destabilizing or stabilizing, respectively ($\Delta G_F^{0,H_2O}$ plots in Fig. S9; $\Delta\Delta G_F^{0,H_2O}$plots in Fig. 3a; complete data in Tables S8 and S9). We obtain a similar distribution of intrinsically stabilizing residues on β11–β15 in both PE and PG, and one highly destabilizing Lys (K^{808}) on β16 (Fig. 3 and S9). Along with the destabilization at the conserved Gly 807 (G^{807}),[15] thermodynamic destabilization at K^{808} bears structural significance in contributing to the C-terminal β16 kink at G^{807} (Fig. 3). Surprisingly, BamA destabilization is more prominent in PE (Fig. 3b left, 3c); furthermore, of the 10 residues that lower β-barrel stability, 7 are localized on the N-terminal strands (β2–β4, β6–β7) (Fig. 3a, b left, 3c and S9). Unlike PE, K^{808} is the sole destabilizing residue in PG (Fig. 3a, b right, 3d and S9), underscoring that membrane composition can selectively alter BamA stability.

Studies have indicated a segregated distribution of PE/PG into local domains in the total *E. coli* membrane.[56,57] Studies also suggest that BamA dynamically interconverts to a "gate laterally-open" state during the templated assembly of a nOMP, through substantial displacement of β1–β5 away from the barrel lumen and into the membrane.[24,25,58,59] BamA also requires less unfolding force in outer membrane vesicles that are PE-enriched.[60] Similarly, we find that PE specifically affects the stability of only the N-terminal residues ($\Delta\Delta G_F^0$ shows 7 of 11 residues as intrinsically destabilizing; Fig. 3b and c) while nearly all the C-terminal residues are stabilizing ($\Delta\Delta G_F^0$ shows only 3 of 23 residues as intrinsically destabilizing; Fig. 3b and c). A similar destabilizing effect is not observed in PG (Fig. 3b and d), wherein nearly all residues are intrinsically stabilizing. By putting together previous findings with our measurements of BamA thermodynamic stability (Fig. 3, S9 and S10), we speculate that the selective destabilization of BamA at the N-terminal strands β2–β7 in PE membranes increases its conformational dynamicity, and may consequently facilitate the interconversion of BamA between the open and closed states for nOMP assembly. Our measurements also reveal a membrane-anchoring function of β8–β15, wherein these residues largely display high $\Delta\Delta G_F^{0,H_2O}$ (−1.32 to −1.87 kcal mol^{-1} in PE; −1.36 to −2.86 kcal mol^{-1} in PG) (Fig. 3, S9; Tables S8 and S9). Therefore, residues of β8-β15 play a thermodynamically stabilizing role. Additionally, intrinsic destabilization of K^{808} mechanically contributes to the inward kink at G^{807}–W^{810} of β16 towards the β-barrel lumen. This β16 kink weakens the β1:β16 seam, enhancing lateral gating. Overall, our results provide

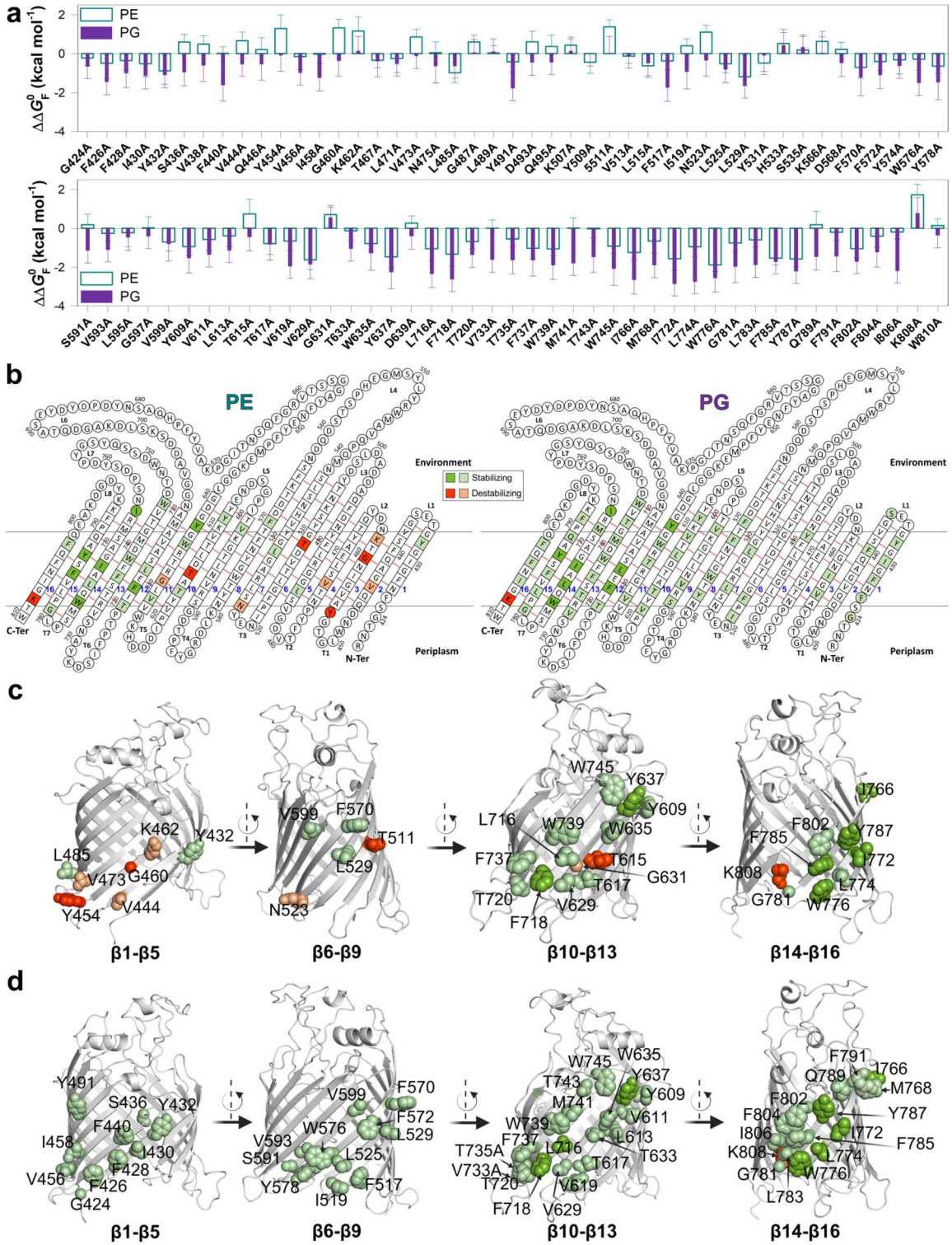

Fig. 3 C-terminal strands anchor folded BamA to the membrane in both PE and PG. (a) Change in $\Delta\Delta G_F^0$ in PC:PE (open histograms, cyan) and PC:PG (filled histograms, purple) upon Xaa → Ala substitution in BamA. Top panel: N-terminal β1–β8; bottom panel: C-terminal β9–β16. N-terminal residues are intrinsically destabilized in PE (top panel). BamA stability is substantially lowered in both PE and PG when C-terminal residues are substituted (bottom panel). Errors are derived from propagation of uncertainty (complete data in Tables S8 and S9). (b) Intrinsically stabilizing (green fills) and destabilizing (red fills) residues of BamA measured from the end-state thermodynamics in PC:PE (left) and PC:PG (right), and highlighted on the two-dimensional topology diagram of the protein. β-Strand numbers are indicated. The results of end-state thermodynamics in PC:PE (c) and PC:PG (d) are also mapped on the structure of BamA (intrinsically stabilizing: green spheres; intrinsically destabilizing: red spheres), and the residues are annotated. Intrinsically destabilizing residues (red) are localized at β2–β4, β6–β7, and β10–β11 of BamA in PC:PE, indicating a dynamic BamA in the PE-rich outer membrane. These residues enhance BamA stability in PG, indicating a more rigid barrel less suitable for its chaperoning function. Residues at the C-terminal strands (β12–β15) stabilize the β-barrel in both membranes. K^{808} in the last strand is intrinsically destabilizing in both membranes.

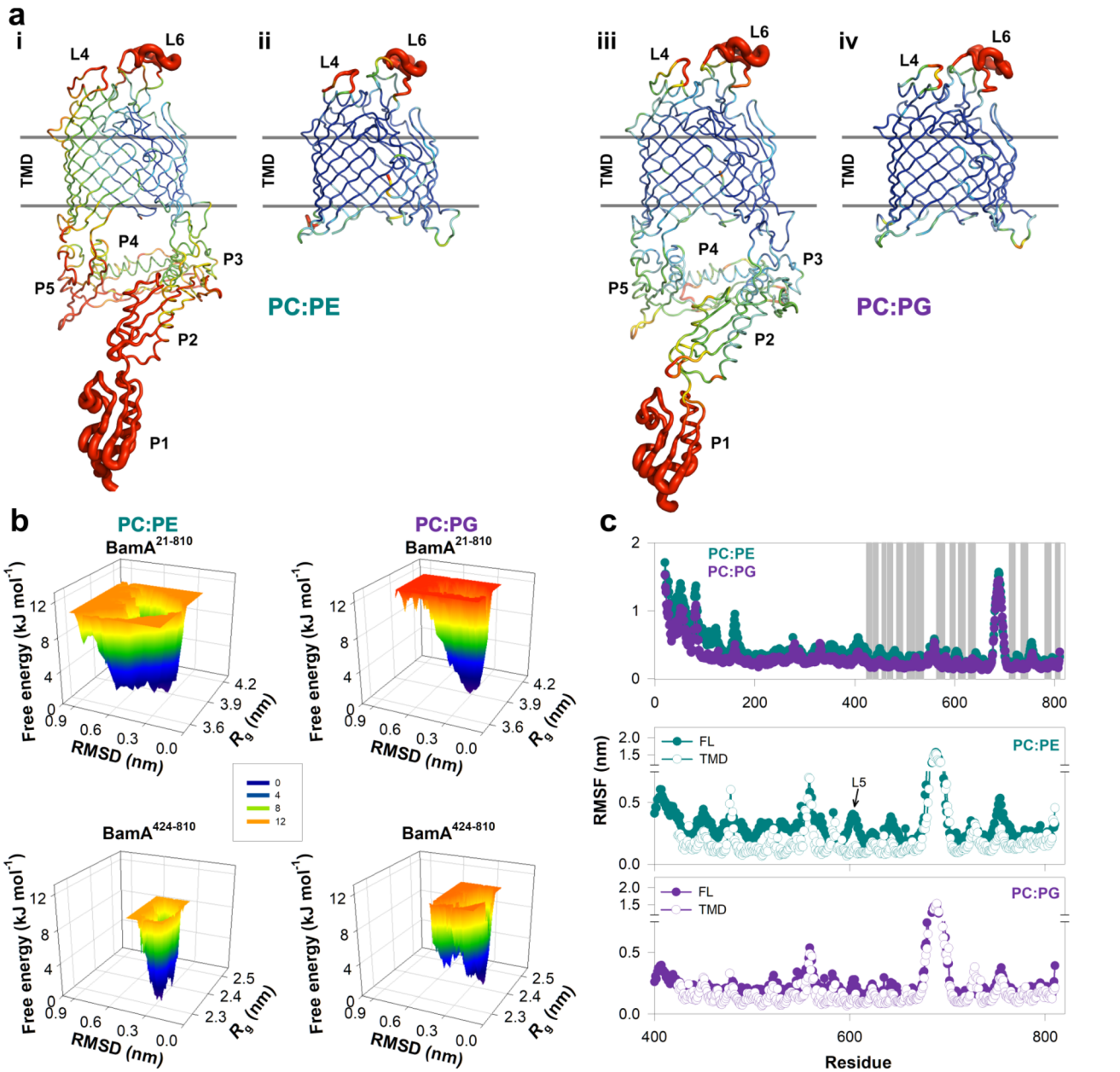

Fig. 4 BamA β-barrel dynamics are regulated by the membrane composition and POTRA. (a) Results of all-atom MD simulations of full-length BamA and POTRA^{-} BamA in PC:PE and PC:PG membranes. Atomic displacement (*B*-factor analysis) is rendered as a sausage representation (red, highest RMSD; dark blue, lowest RMSD). In PC:PE (i), POTRA, L4, and L6 exhibit high structural dynamicity, which allosterically translates to increased dynamicity of N-terminal β3–β6. POTRA deletion abolishes this plasticity in the TMD (ii), limiting the conformational flexibility to L4 and L6. In contrast, PC:PG membranes restrict the conformational dynamicity to only POTRA1 in full-length BamA (iii) and additionally L6 (iii) and (iv). PE increases BamA TMD and POTRA plasticity, while the TMD is conformationally rigid in PG, irrespective of the POTRA. (b, top panels) Free energy landscape (FEL) of full-length BamA (residues 21–810) shows a marked difference in the presence of PC:PE (top left) and PC:PG (top right). Full-length BamA displays greater conformational freedom in PC:PE (higher RMSD; broader FEL profile) than in PC:PG. A narrower FEL profile suggests that PC:PG restricts the β-barrel to concurrently sample fewer conformational ensembles. (b, bottom panels) Removal of the POTRA impacts conformational accessibility of the TMD (BamA$^{424-810}$). The TMD is rigid both in PC:PE and PC:PG (narrower FEL). (c) Comparison of per-residue root-mean-square fluctuation (RMSF) in PC:PE (teal) and PC:PG (purple). Comparison of full-length BamA RMSF in both membranes (top) shows considerable difference in the POTRA region. This is in excellent agreement with the structures in (i) and (iii). β-Strand regions are indicated as gray shading. Comparison of RMSF of full-length and POTRA^{-} BamA in PC:PE (middle) and PC:PG (bottom) shows that the removal of POTRA in BamA$^{424-810}$ decreases fluctuations of the TMD and abolishes fluctuations at loop 5 (residues T^{600}–K^{610}; details in Fig. S14) only in PC:PE (middle). PC:PG (bottom) exerts only a marginal influence on the RMSF, irrespective of whether POTRA is retained. Overall, simulations indicate that PE increases plasticity of the β-barrel domain, and POTRA dynamicity.

a thermodynamic explanation for the structural plasticity of BamA observed in previous studies.[32,59] They also suggest how the higher order of thermodynamic stability in anionic (PG) lipids (Fig. 3b and d) can lower functional efficacy of BamA in PG-rich domains in the bacterial membrane.

BamA exhibits enhanced structural dynamicity in PE membranes

To further determine whether altered structural energetics of BamA in PE-containing membranes affect β-barrel dynamics, we generated full-length BamA embedded PC:PE and PC:PG membranes *in silico* (parameters in Tables S3 and S4 in SI Methods). All-atom molecular dynamics (MD) simulations show that global β-barrel dynamics (RMSD) and per-residue dynamics (RMSF) in full-length BamA are greater in PE than in PG (Fig. 4 and S11–S13). Calculations of the free energy landscape (FEL) additionally support this, wherein we observe greater conformationally accessible structural space for BamA in PE (Fig. 4b, left). Doubling PE levels retains high BamA dynamics (Fig. S12). In contrast, the FEL is narrow in PG (Fig. 4b, right), suggesting that PG can restrict BamA conformational plasticity, allowing formation of fewer structural ensembles (SI movie files 1–5).

Next, we simulated the POTRA-less BamA ($POTRA^{-}$ $BamA^{424–810}$) TMD to understand whether POTRA contributes to this PE- and PG-regulated β-barrel dynamics. Interestingly, POTRA removal substantially lowers the per-residue dynamics in PE (Fig. 4a and c). In particular, the β-barrel becomes conformationally rigid in regions near loops L3, L5, and L6 (preceding the conserved RGF^{663} motif) (Fig. 4c and S14). Fluctuations at L5 are completely abolished, and other loops including L8 show lowered dynamicity. L4 is the only exception, with E^{554}–D^{562} in L4 retaining similar dynamicity despite POTRA truncation. Our MD simulations suggest allosteric POTRA-TMD regulation as vital for BamA dynamicity in PE. POTRAs interact with the membrane through H-bonding with phospholipids, and hydrophobic interactions (*e.g.*, W^{205} and W^{206} in POTRA3 partition to the membrane and establish prolonged contact[61]). Hence, intrinsic POTRA dynamics coupled with POTRA-membrane anchoring interactions can allow the TMD to sample structurally dynamic states, which are vital for its chaperone activity. Unlike PE, the FEL of the $POTRA^{-}$ TMD broadens marginally on PG to accommodate two stable conformational populations (see Fig. S15). We additionally find a marginally greater structural compaction of the β-barrel in PE membranes (R_g ~2.3 nm), when compared with PG (R_g > 2.4 nm) in $POTRA^{-}$ BamA (Fig. S14 and S15). A low RMSF however suggests that all the energetically accessible structures of the BamA TMD in PG have rigid scaffolds, and are delinked from POTRA. Such structural decoupling of the TMD and POTRA impairs BamA function, as seen in a recent study.[62]

To understand if PE increases conformational dynamicity only in BamA, we simulated its mitochondrial homolog Sam50 in PC:PE membranes (Fig. S16 and S17, SI movie files 6 and 7). Interestingly, and unlike BamA, Sam50 displays a lower conformational sampling space than BamA and lower dynamics in its L6 (Fig. S16). However, POTRA deletion shows a similar effect in both systems (Fig. S17). Overall, the interactions we observe between BamA and PE appear specific and are not likely evolutionarily conserved. A comparison of lipid tail order parameters also suggests that the PE- and PG- specific interactions we observe in BamA are highly specific (Fig. S18 and S19).

Our simulations and thermodynamics together provide insights into how TMD and POTRA dynamics, and lipid composition, can influence BamA function. PE membranes support conformational dynamicity of the TMD, which POTRA additionally augments. We propose that these features, along with the highly dynamic β1:β16 seam (aided further by destabilization at K^{808}), allow the BamA TMD to structurally interconvert between the open and closed states within biological timescales for efficient assembly of nOMPs. Our results also suggest that PG can suppress BamA's activity as a chaperone and insertase, by rigidifying the TMD. Overall, we find a lipid-dependent change in dynamicity for the BamA β-barrel, which can regulate its function. *In vivo*, BamA dynamicity may promote its function in PE, with PG suppressing this function. The high dynamicity we observe in the presence of POTRA may be further modulated *in vivo* by BAM lipoproteins, to achieve efficient interactions with the nOMPs.

BamA exhibits parallel folding pathways with a lipid-modulated transition state

The thermodynamic modulation of BamA stability and zonal distribution of BamA dynamics are PE/PG-dependent (Fig. 2–4). Therefore, we next examined whether β-barrel folding is directional, lipid-regulated, and correlates with *in vivo* BAM-assisted assembly. Here, we first monitored early events in BamA (un) folding, by capturing millisecond assembly kinetics in PE and PG using the change in tryptophan fluorescence. Both folding and unfolding are rapid, occur within 60–300 s, and provide rates correlating linearly with [GdnHCl] (Fig. 5a and S20–S24). We fitted the folding kinetics to a quadruple exponential rise function (Fig. S20), and obtained four folding rate constants (k_{f1}, k_{f2}, k_{f3}, and k_{f4}). Unfolding kinetics could be fitted with a double exponential decay function (Fig. S21), providing two unfolding rate constants (k_{u1} and k_{u2}) (Fig. 5a). The observed rates (k_{obs}) together form two characteristic chevron profiles, suggesting that BamA folds *via* two-state transitions that link k_{f1} with k_{u1}, and k_{f3} with k_{u2} (Fig. 5a; see Tables S6 and S7). The two additional rates k_{f2} and k_{f4} in the folding arm did not display a corresponding unfolding rate. They likely represent an unstable kinetic structure that populates only during folding, and may require further characterization.

The observation of two chevron profiles in fast folding kinetics can indicate parallel or sequential pathways of BamA folding. To determine the precise assembly mechanism, we carried out double-jump measurements. We observe that the re-unfolding rate constants of BamA folded in real time (DJ_{RUF} in Fig. 5a and S25) in both PE and PG closely match the respective k_{u1} and k_{u2} from the unfolding kinetics, supporting at least two parallel assembly pathways in both PE and PG. A similar parallel assembly has been observed in *Yersinia* Ail.[53] The total kinetic

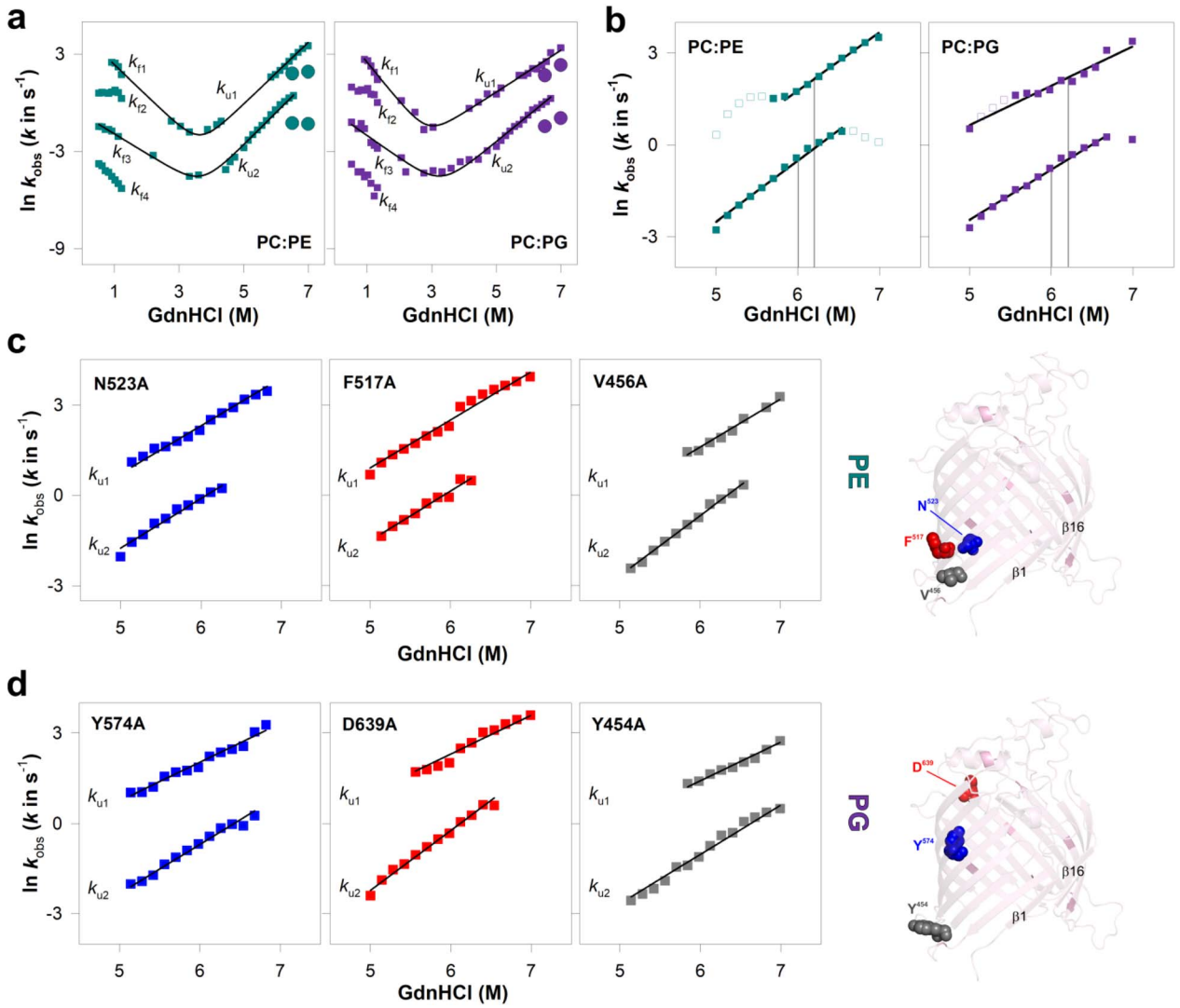

Fig. 5 BamA unfolding is biphasic and proceeds through parallel pathways in PC:PE and PC:PG. (a) Representative folding (k_{f1}, k_{f2}, k_{f3}, and k_{f4}) and unfolding (k_{u1} and k_{u2}) kinetics of BamA monitored using changes in the total fluorescence emission of the 13 intrinsic Trp residues, provide two chevron profiles (fit lines) in both membranes. Each unfolding rate links with two of the folding rates (k_{f1}–k_{u1} and k_{f3}–k_{u2}; fits shown as solid lines), displaying amplitude dependence (see Fig. S22 and S23), and providing the change in kinetic free energy. The folding rates k_{f2} and k_{f4} may correspond to off-pathway events or on-pathway TS structures. At values closer to the C_m, the process is too slow for accurately measuring the rate constants (also see Fig. S22). Interrupted folding (double jump re-unfolding, DJ_{RUF}) measurements (●) display two rates that are in good agreement with k_{u1} and k_{u2} (shown here are rates for t_{age} = 999 s; rates from other t_{age} in Fig. S25), and support BamA (un)folding *via* parallel pathways. (b–d) Unfolding rate constants (k_u values) for WT BamA (b) and its mutants were obtained from fits of the unfolding rates to a linear equation (fits shown as solid lines) using shared m-values (listed in Table S2). (c and d) Unfolding data for three representative BamA variants that are folded (left, blue), unfolded (middle, red), or form non-native interactions (right, gray) in the transition state (TS) structure, in PC:PE (c) and PC:PG (d). The positions of these residues are indicated (right extreme) on the structure of BamA. See Tables S10–S13 for the measured kinetic parameters.

free energy $\Delta G^{0,sum}_{kin}$ from two-state fits of the chevron profiles (-15.21 ± 0.10 kcal mol^{-1} in PE and -12.22 ± 0.15 kcal mol^{-1} in PG) is in good agreement with the $\Delta G^{0,H_2O}_F$ ($\cong -13.0$ kcal mol^{-1}; Fig. 2a), additionally supporting BamA (un) folding through parallel pathways. We obtain similar WT-like chevron profiles for the mutants (Fig. 5b–d and S26), with the total kinetic free energy $\Delta G^{0,sum}_{kin}$ in good agreement with the respective $\Delta G^{0,H_2O}_F$ (Fig. S26, Tables S10 and S11).

We deduced the relative compactness of the transition state (TS, ‡) with respect to the native structure in both pathways and membranes, using the Tanford-β value[63] (β_T). We obtain $\beta_T \cong 0.66$ in the PG-fast pathway, and $\beta_T \cong 0.5$ in PG-slow and PE-fast pathways, suggesting a compact TS ensemble during rapid assembly in PG, and a TS ensemble mid-way between the native structure and unfolded ensemble in the other pathways. Finally, BamA accumulates a diffuse folding nucleus in the PE-slow pathway ($\beta_T \cong 0.37$). Once folded, the unfolding rate constants indicate slower BamA unfolding in PG membranes. This can arise from structural stabilization of the β-barrel that is trapped kinetically by anionic PG. Such structural stabilization also

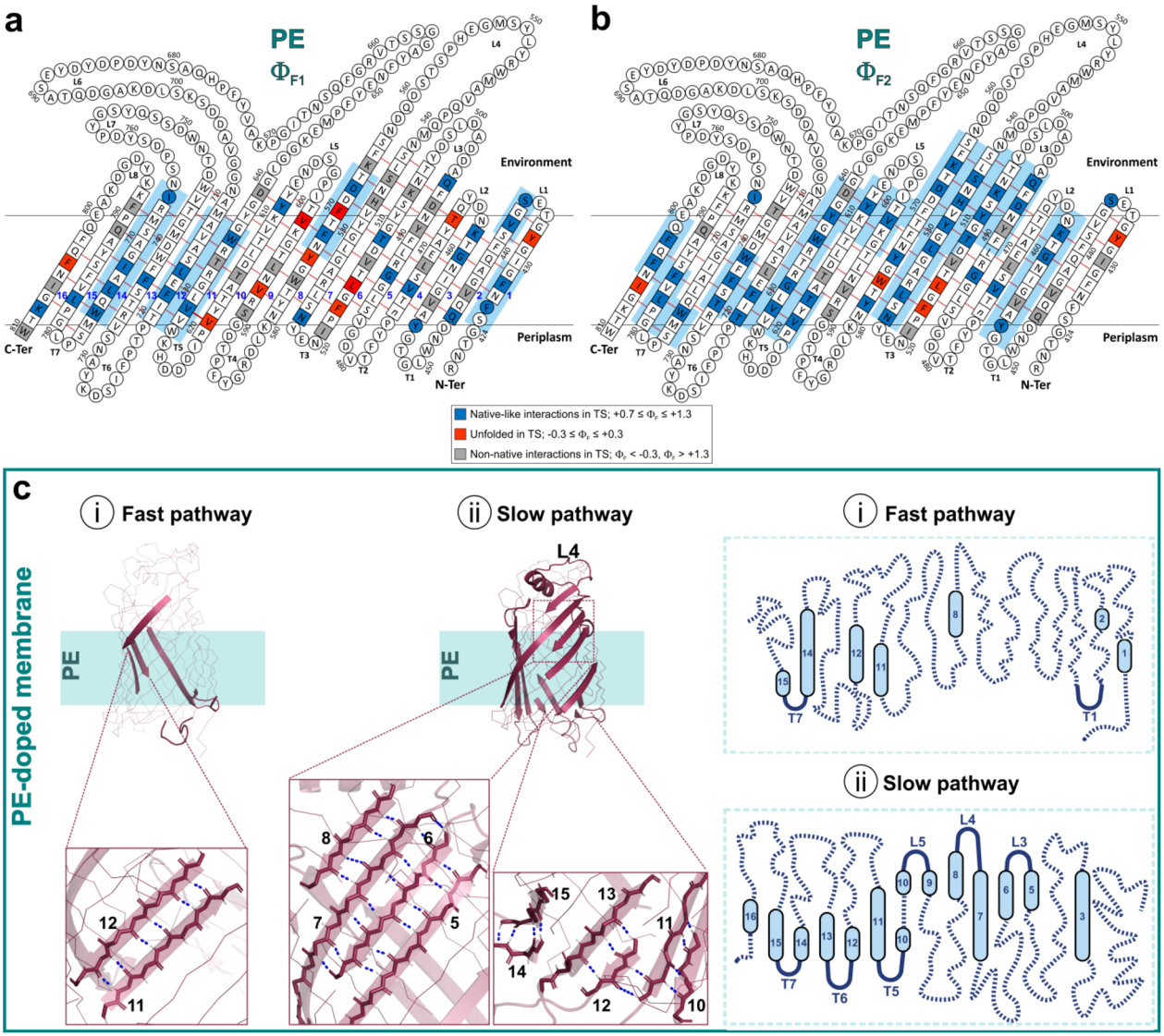

Fig. 6 TS structures formed during BamA folding in PE. (a and b) Two-dimensional topology diagram of BamA highlighting residues that form native-like (blue), unfolded-like (red), or non-native interactions (gray) in the transition state structure of BamA in the fast ($\Phi_{F1\text{-}PE}$) (a) and slow ($\Phi_{F2\text{-}PE}$) (b) pathways. Φ_F ranges used for each color code are indicated below (boxed). β-Strand numbers are annotated in (a) in blue. Residues with $\Delta\Delta G_F^0 \leq -0.09$ kcal mol^{-1} or $\geq +0.09$ kcal mol^{-1} ($\Delta\Delta G_F^0$ > 10% significance) are shown as uppercase single-letter abbreviations. Residues with $\Delta\Delta G_F^0 \leq -0.05$ kcal mol^{-1} or $\geq +0.05$ kcal mol^{-1} ($\Delta\Delta G_F^0$ between 5–9.99%) are in lowercase, italics. To minimize errors in the analyses, mutants with $\Delta\Delta G_F^0$ between ± 0.0499 kcal mol^{-1} were excluded from the topology diagram. Local zones in β-strands which show several native-like interactions are considered folded in the transition state, and are highlighted in light blue casing. Complete data in Fig. S29. (a) The $\Phi_{F1\text{-}PE}$ pathway shows fewer native-like interactions in the transition state, with several residues forming non-native contacts distributed across the β-strands. (b) $\Phi_{F2\text{-}PE}$ displays an assembled β10–β16 towards the periplasmic side of BamA. Additionally, β3–β9 are assembled towards the extracellular face of the β-barrel, suggesting the successful membrane translocation and repositioning of loops L3–L5. (c) Illustrated here are the TS structures we captured in PE. Structures (generated using PyMOL) are presented on the left, and their cartoon representations on the right extreme. PE-rich membranes (pale teal) kinetically retard rapid folding of nBamA, causing minimally structured TS ensembles. The TS ensemble is very poorly structured in the fast pathway (i) with an H-bonded β-hairpin formed only at β11–β12 (left inset), L1, T1, and T7. The TS ensemble is marginally more structured in the slow pathway (ii), with H-bonding at β5–β8 (middle inset), β10–β15 (right inset), L3–L5, and T5–T7. Both pathways involve a structural pattern of transient non-native interactions and unfolded regions formed by nBamA. Several of these interactions are also likely to occur *in vivo* at the membrane interface and BamA^M-bound state.

explains the slow equilibrium profiles BamA achieves in both PE and PG. Overall, both PE and PG influence the TS structures differently, while retaining similar folding pathways. We studied this further using the BamA Xaa → Ala mutants.

PE negatively modulates the BamA folding nucleus to form a collapsed open TS

To deduce structures of the TS structures formed during BamA folding, we captured the unfolding kinetics of the 88 BamA mutant variants in real-time, in both PE and PG membranes

using the change in total Trp fluorescence (10 of the 13 intrinsic Trp are in the TMD; Fig. 1b). Since BamA unfolding shows no detectable intermediate(s), we deduced unfolding rate constants in PE and PG by interpolation (Fig. 5b). Unfolding kinetics of all mutant proteins resembles wild-type BamA, yielding two rate constants. We analyzed the kinetics globally for all proteins (Fig. 5b–d, S27 and S28), wherein we classified the mutants into four groups based on their similar unfolding cooperativity (see Table S2 in SI Methods). Next, we compared the kinetic parameters with wild-type BamA to obtain the kinetic contribution of each side chain ($\Delta\Delta G^{0}_{\ddagger-N}$) during the conversion of the folded (N) protein to its TS (‡). By comparing the kinetic and thermodynamic free energy values at each residue, we obtained parameterized deductions of the TS structures (given by Φ-value analysis[64]) (complete data in Tables S12 and S13), which we then mapped on the two-dimensional topology diagram of BamA (Fig. 6, 7, S29 and S30). As Trp fluorescence has its limitations as a direct reporter of the TS structure, we (i) studied all 88 variants distributed across the 16 β-strands (interface + TMD regions), (ii) carried out global analysis of all kinetic parameters by using only the linear segment of the unfolding arm, and (iii) simplified our interpretation of the Φ-values (obtained for each residue) as regional changes (see below).

To obtain structural details of each TS ensemble, we examined the distribution and contribution of the number and type of residues forming native-like and non-native interactions in each pathway (fast, Φ_{F1}; slow, Φ_{F2}) in PE and PG (Fig. 6, 7. S29 and S30). To simplify our findings from the 88 BamA variants, we annotated β-strand segments that had (i) at least 1–2 residues exhibiting native-like interactions in the TS, and (ii) had <2 residues that were unfolded in the TS in the vicinity, and (iii) had 0–1 residues in the vicinity with non-native interactions in the TS, as folded in the TS (highlighted as pale blue casing in Fig. 6a, b, 7a and b). Interestingly, only $\Phi_{F1\text{-}PE}$ is distinctly different (Fig. 6a). Here, native-like interactions (residues with blue fills) are very few, and correspondingly, non-native interactions (grey fills) are high in number, and distributed across the TMD. This suggests a likely formation of a membrane-adsorbed or off-pathway collapsed state in $\Phi_{F1\text{-}PE}$. We find a similar (local) distribution of non-native interactions across several strands in $\Phi_{F2\text{-}PE}$ (Fig. 6b), suggesting that the zwitterionic PE headgroup negatively influences the local β-strand assembly of BamA.

Further examination of the Φ-values and the topology diagram shows interesting differences in physico-chemical characteristics of residues determining the BamA TS in PE (Fig. 6c, schematics). $\Phi_{F1\text{-}PE}$ has the fewest number (<50%) of residues forming native-like interactions (blue fills), which are clustered at β11–β15, and distributed sparsely across β1–β6. A closer examination of the residues shows that several aromatic residues that play essential membrane-anchoring roles and hydrophobic residues required for β-barrel-acyl tail interaction,[65] are unfolded or form non-native interactions in the TS (complete data in Fig. S29). The observation of several non-native interactions suggests that very few β-strands are structured in $\Phi_{F1\text{-}PE}$. In contrast, the slow folding pathway ($\Phi_{F2\text{-}PE}$) shows formation of native-like interactions across various strands (Fig. 6b and c). Additionally, all interface aromatic residues (except Y^{432}) form near-native interactions early during folding (Fig. S29), and can facilitate membrane anchoring of the BamA β-barrel. Polar side chains of β5–β8 are folded, and β7–β8 are ordered, suggesting the membrane translocation of loops L3–L4 (Fig. 6b and S29). Native-like interactions seen in β11–β15 for $\Phi_{F1\text{-}PE}$ are retained in $\Phi_{F2\text{-}PE}$, and extend to β10 and β16.

The TS structures in PE showed us three important findings: (i) nucleation of folding occurs differently between both fast and slow pathways, (ii) the fast pathway TS is poorly structured (due to several non-native interactions), and (iii) the slow pathway shows native-like interactions that only allow partial BamA structuring at the lower half of the C-terminal strands and the upper half of the N-terminal strands (Fig. 6). Hence, BamA likely undergoes localized folding in PE. The kinetics data reveal that PE inhibits rapid BamA assembly, and triggers hydrophobic collapse of midplane residues, causing the formation of non-native polar contacts. Non-native contacts formed at β5–β8 in the fast pathway can trap L4 and L6 from forming; L4 successfully traverses the bilayer in the slower pathway, nucleating local inter-strand H-bonding in β5–β8 (Fig. 6c). The two locally formed folding nuclei in $\Phi_{F2\text{-}PE}$ (in β5–β8 and β10–β13; Fig. 6b and c) can promote BamA folding through β-barrel closure as one of the last steps in PE membranes. Overall, the absence of a defined directionality for BamA assembly in PE emphasizes the evolutionary requirement of an existing BAM complex as a prerequisite for correct assembly of nascent BamA (nBamA). We also find β5–L4–β8 as a key target zone for designed peptidomimetics to inhibit BamA folding.

Unassisted folding in PG is directed C → N and resembles *in vivo* assembly

In contrast to PE, anionic PG promotes BamA folding. Here, we obtain a greater distribution of native-like interactions across residues (blue fills), with the fewest non-native microstates (grey fills) (Fig. 7a, b and S30). In both $\Phi_{F1\text{-}PG}$ (fast) and $\Phi_{F2\text{-}PG}$ (slow) pathways, a large number of native-like interactions are already established at the C-terminal strands in the TS (Fig. 7a and b, highlighted in pale blue casing). Hence, C-terminal residues populated at β11–β16 are structured in the TS, and are native-like and membrane-anchored, indicating that these β-strands assemble rapidly and before ordering of the other regions of BamA. Therefore, BamA folding in PG proceeds directionally, from C → N-terminal. Such structuring is clearly not seen in either of the pathways in PE, prompting us to interpret that the unassisted folding of BamA in PG resembles the chaperone-mediated C → N assembly seen *in vivo*. TS structures in both pathways share similar microstates and folding energy landscapes, with L4 assembly (rearrangement of β7–β8) and folding of the N-terminal strands occurring late in the pathway.

The fast and slow pathways bifurcate at G^{631} of β11 (Fig. 7a and b). Following early folding nucleation at β12–β16, G^{631} forms non-native contacts in the $\Phi_{F2\text{-}PG}$ (slow) pathway, thereby slowing the membrane transfer of the longest polar loop L6

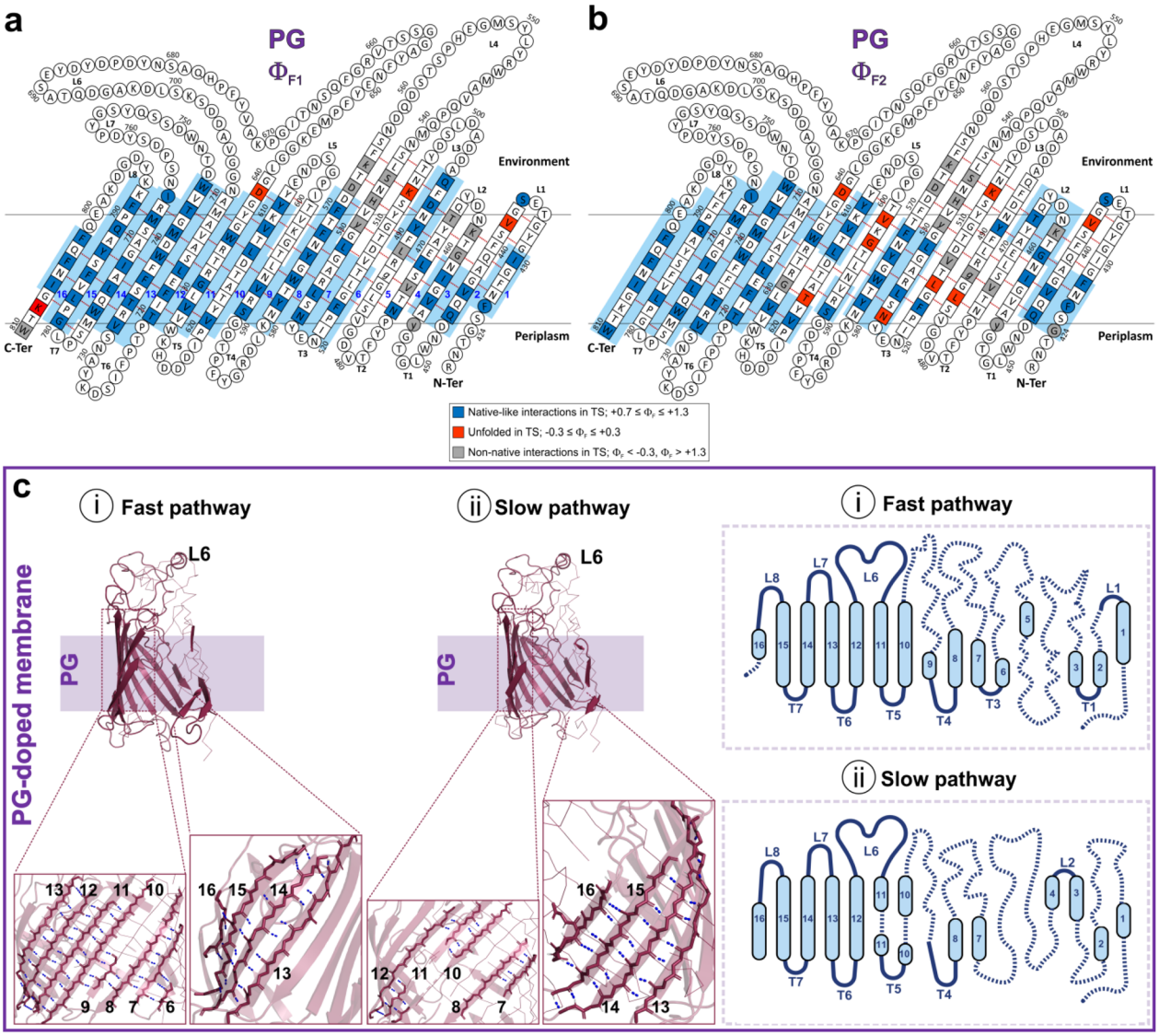

Fig. 7 TS structures formed during BamA folding in PG. (a and b) Two-dimensional topology diagram of BamA highlighting residues that form native-like (blue), unfolded-like (red), or non-native interactions (gray) in the transition state structure of BamA in the fast ($\Phi_{F1\text{-}PG}$) (a) and slow ($\Phi_{F2\text{-}PG}$) (b) pathways. Φ_F ranges used for each color code are indicated below (boxed). β-Strand numbers are annotated in (a) in blue. Residues with $\Delta\Delta G_F^0 \leq -0.09$ kcal mol^{-1} or $\geq +0.09$ kcal mol^{-1} ($\Delta\Delta G_F^0 > 10\%$ significance) are shown as uppercase single-letter abbreviations. Residues with $\Delta\Delta G_F^0 \leq -0.05$ kcal mol^{-1} or $\geq +0.05$ kcal mol^{-1} ($\Delta\Delta G_F^0$ between 5–9.99%) are in lowercase, italics. To minimize errors in the analyses, mutants with $\Delta\Delta G_F^0$ between ± 0.0499 kcal mol^{-1} were excluded from the topology diagram. Local zones in β-strands which show several native-like interactions are considered folded in the transition state, and are highlighted in light blue casing. Complete data in Fig. S30. The two transition states in the fast ($\Phi_{F1\text{-}PG}$) (a) and slow ($\Phi_{F2\text{-}PG}$) (b) pathways show similar assembly structures with the C-terminal strands largely folded. Differences in both pathways largely originate from the correct assembly of G^{631} on β11. In $\Phi_{F1\text{-}PG}$, native-like interactions established by this residue facilitate rapid assembly of BamA by promoting the formation of more native-like interactions at the N-terminal strands (a). However, the non-native interactions formed by G^{631} in $\Phi_{F2\text{-}PG}$ (b) slow BamA assembly in this pathway, which is evident from the several residues distributed across β5–β10 that remain unfolded in the transition state (shown in red) or form non-native interactions (β3–β6; shown in gray). Both TS structures exhibit directional C → N formation of the BamA barrel, similar to the proposed *in vivo* assembly mechanism. (c) Illustrated here are the TS structures we captured in PG. Structures (generated using PyMOL) are presented on the left, and their cartoon diagrams on the right extreme. In PG-rich membranes (pale purple), we obtain a more structured TS for nBamA, with similar native-like interactions at several loci in both fast (i) and slow (ii) pathways. Both pathways share similar structured regions, involving β7–β8, β10–β12, and β13–β16 (insets). Assembled strands also extend from β6–β13 in the fast pathway (i; left insets).

(β11–β12). Furthermore, we find that while ordering of β9–β11 facilitates rapid β-barrel assembly in $\Phi_{F1\text{-}PG}$ (Fig. 7a and c), this zone remains unstructured (transient non-native interactions also formed in β4–β6 at the bilayer midplane) in $\Phi_{F2\text{-}PG}$ (Fig. 7b and c). Additionally, non-native contacts at G^{631} perturb local ordering of β11 in the slow pathway (seen from T^{617}, the H-bonding partner of G^{631}, showing an "unfolded" Φ-value). In turn, this translates to a less-structured β4–β10 (with several

residues unfolded in the TS), and accounts for the lower rates of $\Phi_{F2\text{-}PG}$ in PG membranes. We also find variations in the microstates involving rearrangements in K^{808} and W^{810} of β16 (residues that can help establish the β16 inward kink in folded BamA) in $\Phi_{F1\text{-}PG}$, and the corresponding G^{424} of β1 (facilitates β-barrel closure) in $\Phi_{F2\text{-}PG}$. K^{808} is located in immediate proximity to G^{807}, which is highly conserved from bacterial BamA to mitochondrial Sam50 and chloroplast Toc75 (Figure S31). This local destabilization by K^{808} is essential for G^{807} to adopt unusual ϕ–ψ values required for the inward kink of β16 (Fig. S32).

The large number of native-like interactions (>75%) we measure for BamA in PG, lipid-solvated hydrophobic residues, rapid assembly kinetics, and high β_T values together suggest that PG better supports the intrinsic directional folding for this β-barrel compared to PE, independent of chaperone assistance. The structural and molecular similarity of both TS structures in PG suggests an energetically favorable role for PG in BamA self-assembly. However, the conformational rigidity imposed by PG (when compared to PE) can impede gating motion of BamA and affect its function. Overall, from our observations, we suggest that nBamA displays an intrinsic ability to attain the correctly folded structure in PG membranes over PE membranes, with comparatively less assistance from the BAM complex.

Discussion

Lipid composition induces membrane-specific BamA assembly

Given its indispensable role as a bacterial OMP insertase and its accessibility from the environment, BamA has been considered as one of the most lucrative targets for next-generation designed peptide-based antibiotics. However, our lack of understanding of how BamA folding, stability, and function in the membrane are regulated at the atomic level, has constrained progress in structure-based drug design. Our findings now map (i) residue-level details of how BamA assembles in the membrane (Fig. 6a, b, 7a and b), (ii) TS structures in BamA folding (Fig. 6c and 7c), and (iii) residues essential for the post-folding stability of this membrane protein in PE and PG (Fig. 3). We also identify how mechano-chemical regulatory outcomes can be different for PE and PG lipids on BamA assembly, and its native conformational states. These arise from the differences in lateral packing pressure and headgroup shape (mechanical properties), and lipid ionization state (chemical properties). They cause zonal differences in stability (as seen from equilibrium titrations; Fig. 3), as well as the comparatively higher conformational sampling space and more dynamic BamA in PE (as seen from MD simulations; Fig. 4).

We find a direct kinetic effect of PG in suppressing the β-barrel dynamics vital for BamA's function as a membrane protein chaperone (Fig. 3–4). Here, PG can help folded $BamA^M$ (BamA of the BAM complex) achieve a kinetically stabilized state *in vivo*, and limit its ability to fold nOMPs. In addition, BamE-PG interaction may also sequester BAM islands into PG microdomains[56,66] (see SI notes). The TS structures we map show native-like interactions with well-anchored β-strands formed during BamA directional folding (C-terminal β11–β16 are folded; Fig. 7), supporting C → N assembly of BamA in PG *in vivo*. Furthermore, the negative charge from the PG headgroup and OM lipopolysaccharides,[60] self-association with pre-folded POTRA, and $BamA^M$-mature peptidoglycan[67] interaction, can also promote folding. Such assembly of the nBamA β-barrel can be achieved at the membrane-periplasm interface, with membrane insertion of BamA involving the "swing mechanism" captured in other OMPs.[34] In support of our hypothesis, and our observation of directional BamA assembly in PG, cryoEM conformations of BamA loop deletion variants establish folding of L8 before L5.[31] Such a C → N assembly mechanism also resembles folding of the mitochondrial Tom40 β-barrel.[68] Putting together the kinetic assembly mechanism with the stable end-state BamA–PG assembly (Fig. 3d and 7), and lowered β-barrel dynamics (Fig. 4b), suggests BamA in PG as less susceptible to inhibitors.

Unlike PG, our results show interesting PE-specific differences during BamA folding (Fig. 6). PE retards the spontaneous membrane insertion of BamA, triggering formation of microstates with non-native structures, similar to a physical barrier for rapid BamA folding. PE can also inhibit assembly of other *E. coli* OMPs.[51] Additionally, PE weakens BamA-membrane interaction energetics of the N-terminal strands (Fig. 3b and c). The inhibitory effect of PE on slowing BamA folding allowed us to capture at least two distinct transition state structures BamA adopts during its folding (Fig. 6). The minimal structural and molecular similarity between the two TS ensembles suggests the existence of multipoint structural handles that can be used to target BamA folding. Put together, we find several structural–functional features of BamA in PE, including the partially open TS structures (Fig. 6), weakened membrane-β2–β4 interactions (Fig. 3a–c), highly dynamic β16 with intrinsically destabilized K^{808} (Fig. 3a–c), and kinetically structured L4 (Fig. 6c; discussed later), which can together form excellent target sites for precise sequence-specific inhibitor design.

β9–L5–β10 central to BamA folding-stability-function

Our measurements of BamA thermodynamics (Fig. 3) and assembly kinetics (Fig. 6 and 7) in both PE and PG, suggest that hairpin β9–β10 plays a central demarcating point between N- and C-terminal strand residues, with the presence of unfolded residues in β9–β10 bifurcating both fast and slow pathways. In PE, β9–β10 forms non-native interactions in both pathways; consequently, other interactions at the N- and C-terminal strands are different in both TS structures (Fig. 6). Here, in $\Phi_{F1\text{-}PE}$, the zone comprising S^{591} and L^{595} (in β9) and T^{615} (in β10) forms non-native interactions; V^{593} is unfolded (Fig. 6a). Similarly, in $\Phi_{F2\text{-}PE}$, S^{591} and V^{593} (in β9) and T^{615} (in β10) form non-native interactions (Fig. 6b). Consequently, the cluster of hydrophobic residues at β6–β10, and involving β9–β10, is unfolded in $\Phi_{F1\text{-}PE}$, while the few folded residues at the top (extracellular) region of β9–β10 in $\Phi_{F2\text{-}PE}$ promote local native-like interactions in β7–L4–β8.

The vicinity of β9–β10 also shows differences in Φ_{F1} and Φ_{F2} in PG, with more residues folded in $\Phi_{F1\text{-}PG}$ (Fig. 7a). Here, the

correct assembly of the N-terminal zone in the fast pathway is facilitated by insertion of β9–L5–β10, while the process is stalled in the slow pathway at this hairpin (Fig. 7b). Earlier studies have also implicated BamA-β9 in the formation of a membrane-adsorbed intermediate.[69] Cooperative formation of β-hairpins and H-bonding are the initial steps in nBamA assembly. By associating with pre-folded POTRA, nBamA can form the early structures we map as common to both pathways (Fig. 6 and 7).

Residues at β9–β10 also represent a demarcating hinge between the C-terminal strands that possess intrinsically stabilizing residues, and the destabilized N-terminal strands of BamA in both membranes. Destabilization of β2–β7 and stabilization of β11–β15 of folded BamA in PE (Fig. 3b and c), along with assistance from lipoproteins, can facilitate the interconversion of BamA between the "inward-open" and "laterally-open" states of BamA. This structural interconversion is an important contributor in the folding of a nOMP in the PE-rich bacterial membrane. Our MD simulations also demonstrate that L5 dynamics is lowered remarkably in the absence of POTRA (Fig. 4c), suggesting that β9–β10 can promote allosteric regulation between the two distal extramembranous POTRA and the extracellular L5. Put together, the accumulation of a partially folded (possibly membrane-adsorbed) TS ensemble of BamA stems from mid-barrel (β9–L5–β10) non-native interactions. The likely involvement of β9–β10 in mediating POTRA–L5 interactions, and its role in structural interconversion of the BamA "lateral gate" support this hairpin as an excellent target site for designing BamA-specific peptide-based inhibitors.

Translocation energy barrier and dynamics of extracellular polar loops L4 and L6

A vital energy barrier to complete BamA assembly is the membrane translocation of L4 and L6, and associated charged residues in β7–β8 and β11–β12, respectively. Despite being divergent in sequence and length, L4 carries a conserved YLYS^{551} motif forming a surface-exposed α-helix, with mutations near W^{546}–R^{547} causing lethality.[70,71] L4 residues Q^{540}–L^{549} are highly conserved,[72] and chimeric bactericidal peptidomimetics and the monoclonal antibody MAB1 target E^{554}–H^{555} of L4.[73] Two folding intermediates have been captured in the C → N folding of BamA (β3 and β8–β12) and 26-stranded LptD (β2–β4, L10–L11, and β19).[30,74] The L4 vicinity is not structured in both BamA TS structures and LptD intermediates. Our findings are in excellent agreement with these previous studies, with BamA β8–β12 displaying non-native, partially-folded, or unfolded residues (Fig. 6 and 7), leading to late assembly of L4. We attribute this to a high-energy barrier linked with L4 insertion. L4 is functionally important for BamA.[71,73] We propose that the correct positioning of L4 is consistent with a primary sequence that favors function over rapid scaffold formation. Whether this L4-associated energy barrier of insertion is also key to β9–β16 inserting first during BamA folding *in vivo* remains to be established.

In interesting contrast, L6 does not exhibit a membrane transfer energy barrier, despite being longer and more charged than L4 (26 *versus* 69 residues; 4 *versus* 15R + K + D + E). L6 is also vital for BamA folding and function,[16] with L6 mutations producing conditionally lethal phenotypes with severely reduced BamA levels[16] and growth.[17] L6 positioning is a prerequisite for BamA membrane integration.[47] Its VRGF^{663} motif interacts with conserved residues E^{717} (β12), F^{738} and D^{740} (β13), and G^{771} (β14),[47] establishing a non-covalent interaction network that anchors L6 to the β-barrel lumen. Indeed, G^{771} mutation affects BamA folding.[75] The TS structures in both PE and PG (Fig. 6 and 7) exhibit structured β11–β16, supporting a simultaneous L6 tethering within the β-barrel as an early event in BamA folding. Changes in VRGF^{663} cause assembly defects *in vivo*,[47] supporting a synergistic interaction between β11–L6–β16 for BamA assembly and stability. A similar stabilizing interaction (that helps in loop translocation across the membrane) is absent in L4, explaining the non-native contacts that accumulate at β7–β8 in stalled BamA. The directed membrane translocation of L6, linked with non-native contacts at G^{631}, demarcates both pathways in PG (Fig. 7a and b). This additionally decelerates native H-bonding and strand formation across β4–β10 in the PG-slow pathway. G^{631}, located in β11, is marginally destabilizing in PE (Fig. 3b and c). However, whether stability of the entire β11 strand is altered in BAM, requires further investigation.

Bridging models of BAM-assisted nOMP folding, BamA β-barrel plasticity, and BamA folding

Anfinsen's hypothesis[46] proposed that soluble proteins can achieve their physiologically relevant structures using only the information encoded in their primary sequence. Similarly, we find that the membrane protein BamA can fold spontaneously to attain a thermodynamically stable structure, without requiring assistance from an existing BAM chaperone or lipoproteins. Moreover, features of BamA that we map with our folding kinetics and thermodynamics studies have also been observed in other studies. For example, the C → N assembly that we observe for nBamA in PG membranes has also been demonstrated with BamA^{M} of the BAM complex.[14,25,31,74] Interactions of luminal residues[76] of BamA^{M} observed with N-terminal residues of the incoming nOMP are reflected in the non-native contacts we observe in the TS structures. Such interactions could limit the conformational sampling space of nBamA, while preventing its early membrane release. The membrane insertion of β1–β3 that we map in our TS structures prior to complete folding of β4–β10 (Fig. 6 and 7), could be formed *in vivo* through association with β16-BamA^{M} and possibly membrane thinning. Similar structural intermediates have also been captured with LptD.[30]

We interpret our results in conjunction with the folding pathways captured for other OMPs[37] including BamA^{M} (Fig. 8). While no universal model exists, and further studies are required, we find that a variety of molecular forces (number and strength of local interactions, membrane environment, lipid-mediated conformational sampling, *etc.*) can influence the instantaneous folding process of an incoming nBamA. For example, the distinct PE-specific TS structures and non-native contacts that we detected imply that PE may kinetically retard

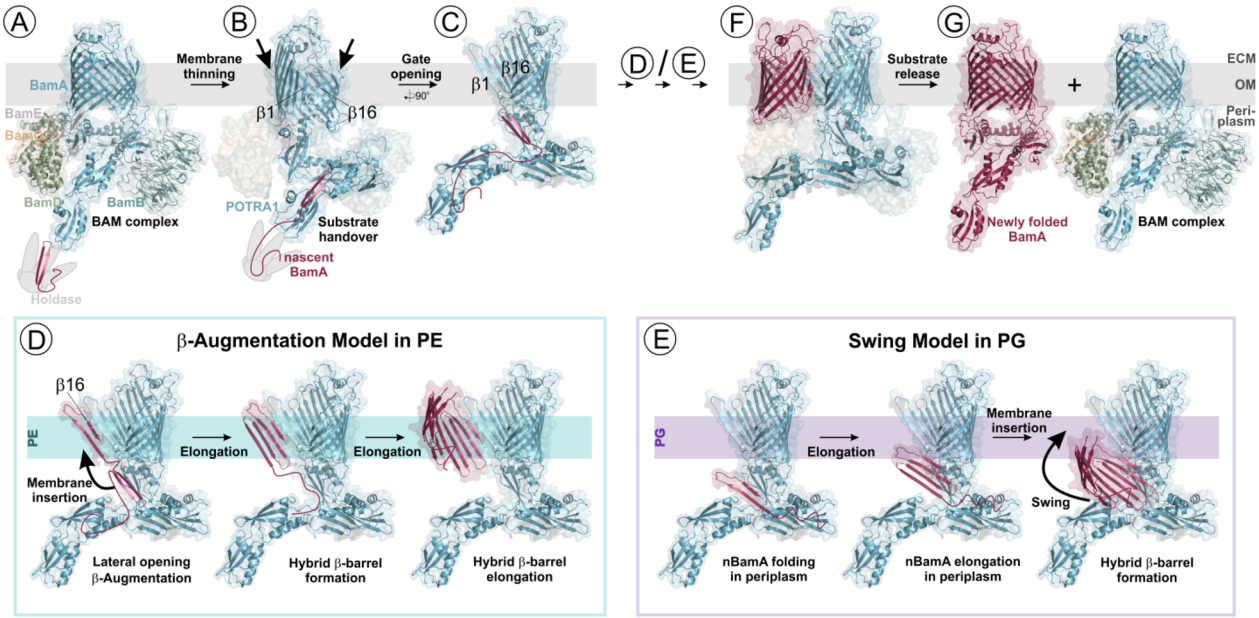

Fig. 8 Integration of a proposed lipid-modulated molecular assembly mechanism of nBamA with its folding *in vivo*. (A) In Gram-negative bacteria, periplasmic holdases such as Skp/SurA (gray) bind to and transport newly synthesized nBamA (maroon) across the periplasm to the BAM complex in the OM. BamA folding is nucleated locally in its Skp/SurA-bound state, prior to its handover to the pre-assembled BAM complex (PDB ID: 7BNQ; $BamA^M$ in cerulean). BamD can also bind to an internal signal in nBamA and promote β-strand formation.[78] (B) Recruitment of BamA to the POTRA/BamB/C/D/E periplasmic ring simultaneously triggers local disruption of the OM and sliding of $BamA^M$ β1 from β16. The latter step converts the "inward open" state ($BamA^M$ β1 and β16 still H-bonded) of $BamA^M$ (A) to the "outward open" state (β1 of $BamA^M$ available to H-bond with the substrate) (B). Together, these changes energetically favor nBamA insertion. (C) Lateral gate opening of $BamA^M$ ("gate wide open" state; shown here without the lipoproteins), where the N-terminal β-strands swing outwards, providing access to nBamA for its C → N directed membrane insertion. Our findings specifically show that this is thermodynamically facilitated by intrinsic destabilization of the N-terminal strands of $BamA^M$, particularly in PE-rich membranes where the BAM complex is highly active. (D/E) Proposed stepwise events in BamA β-strand formation and membrane integration, regulated by its immediate lipidic environment (based on our Φ-value analysis and proposed unassisted folding mechanisms we deduced; see Fig. 6 and 7). BamA can undergo β-augmentation in PE-rich membranes (D), while prefolded BamA swings into the OM in a PG-rich environment (E). (D) The "gate wide open" $BamA^M$ in PE is less stable and highly dynamic at the N-terminal strands. First, nBamA β15–β16 threaded into the $BamA^M$ lumen, forms stable H-bonding with β1 of $BamA^M$. BamA then undergoes β-strand elongation resembling the β-augmentation model.[74,79] The relatively slower folding of BamA in the presence of PE (D), coupled with SurA/Skp assistance, POTRA-mediated hand-off, and BAM complex assistance, can ensure that (i) unfolded protein in the periplasm does not insert into the inner membrane, which is also PE-rich, (ii) off-pathway irreversible structures in the membrane are not adopted after SurA/Skp hand-off, and (iii) the assembly is completed correctly after binding of lipoproteins. (E) In PG-rich local environments, a conformationally restricted $BamA^M$ can promote nBamA structuring primarily in the periplasmic ring, membrane interface, and in the POTRA-lipoprotein-bound states. Interaction of nBamA with $BamA^M$-β1 occurs as one of the last events during folding after near-complete β-strand formation. β-Barrel assembly at the C-terminal and mid-barrel zones trigger membrane insertion of BamA following a swing mechanism.[34] In PG, $BamA^M$ could primarily assist in β7–β8 assembly, wherein membrane translocation of L4 presents an energy barrier and occurs late in the folding process. We propose that the non-native interactions we observed at the N-terminus of BamA correspond to regions where nBamA is in contact with $BamA^M$ during assembly, as seen in the lumen-catalyzed model.[76] (F) Membrane insertion of all the β-strands of BamA and hybrid nBamA–$BamA^M$ formation (PDB ID: 6V05) eventually triggers β-barrel closure through β1–β16 association (intra-barrel H-bonding) of the respective polypeptides, ultimately releasing the newly formed BamA from $BamA^M$ and into the membrane (G). All TS structures were rendered in PyMOL and assembled using CorelDraw.

BamA folding *in vivo*. Hence, under physiological conditions, nBamA must engage $BamA^M$ in the OM for proper assembly, which would, in turn, suppress the formation of the off-pathway structures we see in $\Phi_{F1\text{-}PE}$ (Fig. 6). Furthermore, we find that folded BamA is more dynamic in PE with intrinsically destabilized N-terminal residues (Fig. 3 and 4), which would enhance its function as an OM chaperone. Putting these observations together, we propose that nBamA may adopt a β-augmentation[74]–like mechanism in PE-rich membrane environments. Here, β15–β16 of nBamA can associate with β1 of $BamA^M$ while in the membrane interface or the periplasm (Fig. 8A–C), which then orchestrates β-strand formation; β-strand elongation can also proceed after membrane insertion, as seen for LptD through β-augmentation,[74] transiently forming a hybrid β-barrel in the OM (Fig. 8D).

In contrast to PE, we see that PG promotes BamA folding by accelerating membrane adsorption and β-strand formation, with the TS closely resembling the native state (Fig. 7). *In vivo*, this could make nBamA likely dependent on $BamA^M$ primarily for membrane insertion (Fig. 8E). Furthermore, our stability and MD simulation studies (Fig. 3 and 4) show that BamA is more rigid in PG, which may lower its efficacy as an OM chaperone. Based on these findings, we hypothesize that in a PG-rich local environment *in vivo*, the overall folding pathway of nBamA could follow the swing model (Fig. 8E) proposed for EspP.[25,34] Here, nBamA could acquire substantial β-strand structuring at

the C-terminal strands through association with the PG headgroup; this partially-folded nBamA can then associate with the lateral gate of a conformationally restricted $BamA^{M}$, which then acts as a molecular hinge to facilitate its membrane insertion.

We find non-native interactions populated in β7–L4–β8 to be common in three of the four TS structures (Fig. 6 and 7). These likely represent interactions formed with the $BamA^{M}$ lumen, as proposed in the lumen-catalyzed model for LptD.[76] The lipid-dependent assemblies we obtain for the four TS structures (illustrated in Fig. 6c, 7c, 8D and E) appear to bear (i) mechanistic similarity to the general BAM–assisted folding *in vivo*, (ii) similarities to features of three proposed folding models (β-augmentation, swing, and lumen-catalyzed models),[37] and (iii) correlation with the protein–bilayer interaction energetics of the native well-folded BamA. These and other mechanisms can co-occur *in vivo*, or as mutually exclusive events, and will require a direct measurement of BamA folding in live bacteria.

The ability of BamA to display directionality in its *in vitro* assembly suggests the co-evolution of the protein's primary sequence with its assembly machinery. Our findings are supported by previous reports, wherein residues mutated in antibiotic resistant strains are not involved in BamA stability,[37] suggesting the importance of stabilizing residues in BamA function *in vivo*. Lipids also play a key role in BamA dynamics and function. Our results suggest how BamA responds to its surrounding lipids, with lipid-dependent differences in BamA folding and TMD stability. Therefore, we propose that nBamA folding may follow divergent routes *in vivo*. BamA has been rarely studied as the substrate OMP in BAM-assisted folding studies (see SI notes) and would greatly benefit from *in vivo* characterization. Our study shows that PG promotes BamA folding, which raises the question of how nBamA folding is intercepted *in vivo* where PG contents are at 15–20% in the OM inner leaflet, and higher in PG-rich lipid domains. Clearly, nBamA folding would also be directly modulated by other factors, such as periplasmic chaperones and the BAM lipoproteins, requiring detailed investigations. It would be of interest to further examine how our observations of BamA folding mechanisms and stabilizing factors display sequence specificity across various ESKAPEE pathogens.

Conclusions

Antibiotic resistance is now a severe and emerging crisis, given the increased threat of newer and more potent variants of ESKAPEE pathogens. An immediate need is for thorough exploration of existing high-priority target proteins that are (i) essential and unique to the bacterium and (ii) readily accessible from the external environment.[2] BamA meets both criteria of accessibility and essentiality, cementing it as a central molecule for knowledge-based design of next-generation antimicrobial peptides and drugs. By characterizing the thermodynamics of BamA folding and stability in detail, we have obtained meaningful insights into how BamA dynamics and function are regulated by the membrane. Furthermore, we show residue-level changes in BamA stability. Additionally, we have identified β5–L4–β8, β9–L5–β10, and β16-K^{808} (located in proximity to the conserved G^{807}; Fig. S31 and S32) as lucrative target sites for designing BamA inhibitors. Our work represents an important milestone in identifying potential target zones in addition to the β-barrel seam, both for BamA function and nBamA folding. Such knowledge-based development of protein-specific silencers (*e.g.*, peptidomimetics) as promising interventions can lead to effective therapeutic strategies for antimicrobial resistance.

Author contributions

RM conceived, designed and supervised the study, acquired funding, conceived experimental designs, analyzed and interpreted the results, generated figures, and wrote and edited the manuscript. AG contributed to screening experiments, performed the kinetics experiments, simulations, data analysis, and generated the figures. AG, AMR, AGP, and VK carried out mutant library generation (DNA and protein), and equilibrium titrations. AMR contributed to data analysis of equilibrium experiments. AGP contributed to generating the figures. VK performed screening experiments.

Conflicts of interest

The authors declare no competing interests (financial and non-financial) with the contents of this article.

Data availability

The authors declare that the data supporting the findings of this study are available within the paper and its supplementary information (SI). Should any raw data files be needed in another format, they are available from the corresponding author. Supplementary information: SI file with complete methods, SI notes, SI figures and tables, additional supporting data, source data, SI references and movie files 1–7. See DOI: https://doi.org/10.1039/d5sc07027a.

Acknowledgements

AG thanks IISER Bhopal for a research fellowship. AGP thanks University Grants Commission (UGC), India for a research fellowship. RM is a Wellcome Trust – DBT India Alliance Senior Fellow. The authors thank Deepti Chaturvedi for cloning the gene and Sapna Choudhary for technical assistance. This work was supported by the Lady Tata Memorial Trust (LTMT), and in part by the Department of Biotechnology grant HRD-20/1/2024-HRD-DBT and Science and Engineering Research Board grant EMR/2016/001774, to RM.

References

1 A. Tarasenko, B. N. Papudeshi, S. R. Grigson, V. Mallawaarachchi, A. L. K. Hutton, M. S. Warner, J. J. Barr, J. Iredell, B. Eijkelkamp and R. A. Edwards, Reprogramming resistance: phage-antibiotic synergy

targets efflux systems in ESKAPEE pathogens, *mBio*, 2025, **16**, e0182225.
2 T. M. Privalsky, A. M. Soohoo, J. Wang, C. T. Walsh, G. D. Wright, E. M. Gordon, N. S. Gray and C. Khosla, Prospects for Antibacterial Discovery and Development, *J. Am. Chem. Soc.*, 2021, **143**, 21127–21142.
3 S. W. Cowan, T. Schirmer, G. Rummel, M. Steiert, R. Ghosh, R. A. Pauptit, J. N. Jansonius and J. P. Rosenbusch, Crystal structures explain functional properties of two E. coli porins, *Nature*, 1992, **358**, 727–733.
4 A. D. Ferguson, E. Hofmann, J. W. Coulton, K. Diederichs and W. Welte, Siderophore-mediated iron transport: crystal structure of FhuA with bound lipopolysaccharide, *Science*, 1998, **282**, 2215–2220.
5 J. M. Rutz, J. Liu, J. A. Lyons, J. Goranson, S. K. Armstrong, M. A. McIntosh, J. B. Feix and P. E. Klebba, Formation of a gated channel by a ligand-specific transport protein in the bacterial outer membrane, *Science*, 1992, **258**, 471–475.
6 T. Schirmer, T. A. Keller, Y. F. Wang and J. P. Rosenbusch, Structural basis for sugar translocation through maltoporin channels at 3.1 A resolution, *Science*, 1995, **267**, 512–514.
7 D. Jeanteur, T. Schirmer, D. Fourel, V. Simonet, G. Rummel, C. Widmer, J. P. Rosenbusch, F. Pattus and J. M. Pages, Structural and functional alterations of a colicin-resistant mutant of OmpF porin from Escherichia coli, *Proc. Natl. Acad. Sci. U. S. A.*, 1994, **91**, 10675–10679.
8 M. Olesky, S. Zhao, R. L. Rosenberg and R. A. Nicholas, Porin-mediated antibiotic resistance in Neisseria gonorrhoeae: ion, solute, and antibiotic permeation through PIB proteins with penB mutations, *J. Bacteriol.*, 2006, **188**, 2300–2308.
9 T. Wu, J. Malinverni, N. Ruiz, S. Kim, T. J. Silhavy and D. Kahne, Identification of a multicomponent complex required for outer membrane biogenesis in *Escherichia coli*, *Cell*, 2005, **121**, 235–245.
10 R. Voulhoux, M. P. Bos, J. Geurtsen, M. Mols and J. Tommassen, Role of a highly conserved bacterial protein in outer membrane protein assembly, *Science*, 2003, **299**, 262–265.
11 J. Werner and R. Misra, YaeT (Omp85) affects the assembly of lipid-dependent and lipid-independent outer membrane proteins of *Escherichia coli*, *Mol. Microbiol.*, 2005, **57**, 1450–1459.
12 S. H. Cho, J. Szewczyk, C. Pesavento, M. Zietek, M. Banzhaf, P. Roszczenko, A. Asmar, G. Laloux, A. K. Hov, P. Leverrier, C. Van der Henst, D. Vertommen, A. Typas and J. F. Collet, Detecting envelope stress by monitoring beta-barrel assembly, *Cell*, 2014, **159**, 1652–1664.
13 A. M. Plummer and K. G. Fleming, BamA Alone Accelerates Outer Membrane Protein Folding *In Vitro* through a Catalytic Mechanism, *Biochemistry*, 2015, **54**, 6009–6011.
14 P. B. Tiwari and R. Mahalakshmi, Interplay of protein primary sequence, lipid membrane, and chaperone in beta-barrel assembly, *Protein Sci.*, 2021, **30**, 624–637.
15 K. Lundquist, J. Bakelar, N. Noinaj and J. C. Gumbart, C-terminal kink formation is required for lateral gating in BamA, *Proc. Natl. Acad. Sci. U. S. A.*, 2018, **115**, E7942–E7949.
16 M. Leonard-Rivera and R. Misra, Conserved residues of the putative L6 loop of Escherichia coli BamA play a critical role in the assembly of beta-barrel outer membrane proteins, including that of BamA itself, *J. Bacteriol.*, 2012, **194**, 4662–4668.
17 N. Noinaj, A. J. Kuszak, J. C. Gumbart, P. Lukacik, H. Chang, N. C. Easley, T. Lithgow and S. K. Buchanan, Structural insight into the biogenesis of beta-barrel membrane proteins, *Nature*, 2013, **501**, 385–390.
18 A. Luther, M. Urfer, M. Zahn, M. Muller, S. Y. Wang, M. Mondal, A. Vitale, J. B. Hartmann, T. Sharpe, F. L. Monte, H. Kocherla, E. Cline, G. Pessi, P. Rath, S. M. Modaresi, P. Chiquet, S. Stiegeler, C. Verbree, T. Remus, M. Schmitt, C. Kolopp, M. A. Westwood, N. Desjonqueres, E. Brabet, S. Hell, K. LePoupon, A. Vermeulen, R. Jaisson, V. Rithie, G. Upert, A. Lederer, P. Zbinden, A. Wach, K. Moehle, K. Zerbe, H. H. Locher, F. Bernardini, G. E. Dale, L. Eberl, B. Wollscheid, S. Hiller, J. A. Robinson and D. Obrecht, Chimeric peptidomimetic antibiotics against Gram-negative bacteria, *Nature*, 2019, **576**, 452–458.
19 P. Rath, A. Hermann, R. Schaefer, E. Agustoni, J. M. Vonach, M. Siegrist, C. Miscenic, A. Tschumi, D. Roth, C. Bieniossek and S. Hiller, High-throughput screening of BAM inhibitors in native membrane environment, *Nat. Commun.*, 2023, **14**, 5648.
20 J. J. Psonis, P. Chahales, N. S. Henderson, N. W. Rigel, P. S. Hoffman and D. G. Thanassi, The small molecule nitazoxanide selectively disrupts BAM-mediated folding of the outer membrane usher protein, *J. Biol. Chem.*, 2019, **294**, 14357–14369.
21 Y. Imai, K. J. Meyer, A. Iinishi, Q. Favre-Godal, R. Green, S. Manuse, M. Caboni, M. Mori, S. Niles, M. Ghiglieri, C. Honrao, X. Ma, J. J. Guo, A. Makriyannis, L. Linares-Otoya, N. Bohringer, Z. G. Wuisan, H. Kaur, R. Wu, A. Mateus, A. Typas, M. M. Savitski, J. L. Espinoza, A. O'Rourke, K. E. Nelson, S. Hiller, N. Noinaj, T. F. Schaberle, A. D'Onofrio and K. Lewis, A new antibiotic selectively kills Gram-negative pathogens, *Nature*, 2019, **576**, 459–464.
22 M. G. K. Ghequire, T. Swings, J. Michiels, S. K. Buchanan and R. De Mot, Hitting with a BAM: Selective Killing by Lectin-Like Bacteriocins, *mBio*, 2018, **9**, e02138–02117.
23 J. B. Hartmann, M. Zahn, I. M. Burmann, S. Bibow and S. Hiller, Sequence-Specific Solution NMR Assignments of the beta-Barrel Insertase BamA to Monitor Its Conformational Ensemble at the Atomic Level, *J. Am. Chem. Soc.*, 2018, **140**, 11252–11260.
24 M. G. Iadanza, A. J. Higgins, B. Schiffrin, A. N. Calabrese, D. J. Brockwell, A. E. Ashcroft, S. E. Radford and N. A. Ranson, Lateral opening in the intact beta-barrel assembly machinery captured by cryo-EM, *Nat. Commun.*, 2016, **7**, 12865.
25 M. T. Doyle, J. R. Jimah, T. Dowdy, S. I. Ohlemacher, M. Larion, J. E. Hinshaw and H. D. Bernstein, Cryo-EM structures reveal multiple stages of bacterial outer membrane protein folding, *Cell*, 2022, **185**, 1143–1156.

26 D. Sun, K. M. Storek, D. Tegunov, Y. Yang, C. P. Arthur, M. Johnson, J. G. Quinn, W. Liu, G. Han, H. S. Girgis, M. K. Alexander, A. K. Murchison, S. Shriver, C. Tam, H. Ijiri, H. Inaba, T. Sano, H. Yanagida, J. Nishikawa, C. E. Heise, W. J. Fairbrother, M. W. Tan, N. Skelton, W. Sandoval, B. D. Sellers, C. Ciferri, P. A. Smith, P. C. Reid, C. N. Cunningham, S. T. Rutherford and J. Payandeh, The discovery and structural basis of two distinct state-dependent inhibitors of BamA, *Nat. Commun.*, 2024, **15**, 8718.

27 L. R. Warner, P. Z. Gatzeva-Topalova, P. A. Doerner, A. Pardi and M. C. Sousa, Flexibility in the Periplasmic Domain of BamA Is Important for Function, *Structure*, 2017, **25**, 94–106.

28 P. A. Doerner and M. C. Sousa, Extreme Dynamics in the BamA beta-Barrel Seam, *Biochemistry*, 2017, **56**, 3142–3149.

29 C. L. Hagan, D. B. Westwood and D. Kahne, bam Lipoproteins Assemble BamA *in vitro*, *Biochemistry*, 2013, **52**, 6108–6113.

30 T. M. A. Dos Santos, B. D. Thomson, M. D. Marquez, L. Pan, T. H. Monfared and D. E. Kahne, Native beta-barrel substrates pass through two shared intermediates during folding on the BAM complex, *Proc. Natl. Acad. Sci. U. S. A.*, 2024, **121**, e2409672121.

31 D. Tomasek, S. Rawson, J. Lee, J. S. Wzorek, S. C. Harrison, Z. Li and D. Kahne, Structure of a nascent membrane protein as it folds on the BAM complex, *Nature*, 2020, **583**, 473–478.

32 C. Shen, S. Chang, Q. Luo, K. C. Chan, Z. Zhang, B. Luo, T. Xie, G. Lu, X. Zhu, X. Wei, C. Dong, R. Zhou, X. Zhang, X. Tang and H. Dong, Structural basis of BAM-mediated outer membrane beta-barrel protein assembly, *Nature*, 2023, **617**, 185–193.

33 P. White, S. F. Haysom, M. G. Iadanza, A. J. Higgins, J. M. Machin, J. M. Whitehouse, J. E. Horne, B. Schiffrin, C. Carpenter-Platt, A. N. Calabrese, K. M. Storek, S. T. Rutherford, D. J. Brockwell, N. A. Ranson and S. E. Radford, The role of membrane destabilisation and protein dynamics in BAM catalysed OMP folding, *Nat. Commun.*, 2021, **12**, 4174.

34 M. T. Doyle and H. D. Bernstein, Bacterial outer membrane proteins assemble *via* asymmetric interactions with the BamA beta-barrel, *Nat. Commun.*, 2019, **10**, 3358.

35 L. Han, J. Zheng, Y. Wang, X. Yang, Y. Liu, C. Sun, B. Cao, H. Zhou, D. Ni, J. Lou, Y. Zhao and Y. Huang, Structure of the BAM complex and its implications for biogenesis of outer-membrane proteins, *Nat. Struct. Mol. Biol.*, 2016, **23**, 192–196.

36 X. Wang, J. H. Peterson and H. D. Bernstein, Bacterial Outer Membrane Proteins Are Targeted to the Bam Complex by Two Parallel Mechanisms, *mBio*, 2021, **12**, e00597–00521.

37 A. George, A. G. Patil and R. Mahalakshmi, ATP-independent assembly machinery of bacterial outer membranes: BAM complex structure and function set the stage for next-generation therapeutics, *Protein Sci.*, 2024, **33**, e4896.

38 R. D. Miller, A. Iinishi, S. M. Modaresi, B. K. Yoo, T. D. Curtis, P. J. Lariviere, L. Liang, S. Son, S. Nicolau, R. Bargabos, M. Morrissette, M. F. Gates, N. Pitt, R. P. Jakob, P. Rath, T. Maier, A. G. Malyutin, J. T. Kaiser, S. Niles, B. Karavas, M. Ghiglieri, S. E. J. Bowman, D. C. Rees, S. Hiller and K. Lewis, Computational identification of a systemic antibiotic for gram-negative bacteria, *Nat. Microbiol.*, 2022, **7**, 1661–1672.

39 E. M. Hart, A. M. Mitchell, A. Konovalova, M. Grabowicz, J. Sheng, X. Han, F. P. Rodriguez-Rivera, A. G. Schwaid, J. C. Malinverni, C. J. Balibar, S. Bodea, Q. Si, H. Wang, M. F. Homsher, R. E. Painter, A. K. Ogawa, H. Sutterlin, T. Roemer, T. A. Black, D. M. Rothman, S. S. Walker and T. J. Silhavy, A small-molecule inhibitor of BamA impervious to efflux and the outer membrane permeability barrier, *Proc. Natl. Acad. Sci. U. S. A.*, 2019, **116**, 21748–21757.

40 M. E. Walker, W. Zhu, J. H. Peterson, H. Wang, J. Patteson, A. Soriano, H. Zhang, T. Mayhood, Y. Hou, S. Mesbahi-Vasey, M. Gu, J. Frost, J. Lu, J. Johnston, C. Hipolito, S. Lin, R. E. Painter, D. Klein, A. Walji, A. Weinglass, T. M. Kelly, A. Saldanha, J. Schubert, H. D. Bernstein and S. S. Walker, Antibacterial macrocyclic peptides reveal a distinct mode of BamA inhibition, *Nat. Commun.*, 2025, **16**, 3395.

41 M. Georgieva, F. Stojceski, F. Wuthrich, C. Sosthene, L. Blanco Perez, G. Grasso and N. Jacquier, Mutations in the essential outer membrane protein BamA contribute to Escherichia coli resistance to the antimicrobial peptide TAT-RasGAP(317-326), *J. Biol. Chem.*, 2025, **301**, 108018.

42 Y. Wang, Y. Cheng, Y. Li and X. Fu, Rationally Designed Self-Derived Peptides Kill *Escherichia coli* by Targeting BamA and BamD Essential for Outer Membrane Protein Biogenesis, *ACS Infect. Dis.*, 2025, **11**, 1092–1103.

43 A. M. Woodard, F. Peccati, C. D. Navo, G. Jimenez-Oses and D. A. Mitchell, Darobactin Substrate Engineering and Computation Show Radical Stability Governs Ether *versus* C–C Bond Formation, *J. Am. Chem. Soc.*, 2024, **146**, 14328–14340.

44 M. Nesic, D. B. Ryffel, J. Maturano, M. Shevlin, S. R. Pollack, D. R. Gauthier Jr, P. Trigo-Mourino, L. K. Zhang, D. M. Schultz, J. M. McCabe Dunn, L. C. Campeau, N. R. Patel, D. A. Petrone and D. Sarlah, Total Synthesis of Darobactin A, *J. Am. Chem. Soc.*, 2022, **144**, 14026–14030.

45 F. Schneider, Y. Guo, Y. C. Lin, K. J. Eberle, D. Chiodi, J. A. Greene, C. Lu and P. S. Baran, Total Synthesis of Dynobactin A, *J. Am. Chem. Soc.*, 2024, **146**, 6444–6448.

46 C. B. Anfinsen, Principles that govern the folding of protein chains, *Science*, 1973, **181**, 223–230.

47 J. S. Wzorek, J. Lee, D. Tomasek, C. L. Hagan and D. E. Kahne, Membrane integration of an essential beta-barrel protein prerequires burial of an extracellular loop, *Proc. Natl. Acad. Sci. U. S. A.*, 2017, **114**, 2598–2603.

48 G. J. Patel and J. H. Kleinschmidt, The lipid bilayer-inserted membrane protein BamA of *Escherichia coli* facilitates insertion and folding of outer membrane protein A from its complex with Skp, *Biochemistry*, 2013, **52**, 3974–3986.

49 B. Schiffrin, A. N. Calabrese, A. J. Higgins, J. R. Humes, A. E. Ashcroft, A. C. Kalli, D. J. Brockwell and S. E. Radford, Effects of Periplasmic Chaperones and

Membrane Thickness on BamA-Catalyzed Outer-Membrane Protein Folding, *J. Mol. Biol.*, 2017, **429**, 3776–3792.
50 J. E. Horne, D. J. Brockwell and S. E. Radford, Role of the lipid bilayer in outer membrane protein folding in Gram-negative bacteria, *J. Biol. Chem.*, 2020, **295**, 10340–10367.
51 D. Gessmann, Y. H. Chung, E. J. Danoff, A. M. Plummer, C. W. Sandlin, N. R. Zaccai and K. G. Fleming, Outer membrane beta-barrel protein folding is physically controlled by periplasmic lipid head groups and BamA, *Proc. Natl. Acad. Sci. U. S. A.*, 2014, **111**, 5878–5883.
52 G. J. Patel, S. Behrens-Kneip, O. Holst and J. H. Kleinschmidt, The periplasmic chaperone Skp facilitates targeting, insertion, and folding of OmpA into lipid membranes with a negative membrane surface potential, *Biochemistry*, 2009, **48**, 10235–10245.
53 A. George, R. Ravi, P. B. Tiwari, S. R. Srivastava, V. Jain and R. Mahalakshmi, Engineering a Hyperstable Yersinia pestis Outer Membrane Protein Ail Using Thermodynamic Design, *J. Am. Chem. Soc.*, 2022, **144**, 1545–1555.
54 R. E. Jefferson, T. M. Blois and J. U. Bowie, Membrane proteins can have high kinetic stability, *J. Am. Chem. Soc.*, 2013, **135**, 15183–15190.
55 H. Hong and L. K. Tamm, Elastic coupling of integral membrane protein stability to lipid bilayer forces, *Proc. Natl. Acad. Sci. U. S. A.*, 2004, **101**, 4065–4070.
56 S. Vanounou, A. H. Parola and I. Fishov, Phosphatidylethanolamine and phosphatidylglycerol are segregated into different domains in bacterial membrane. A study with pyrene-labelled phospholipids, *Mol. Microbiol.*, 2003, **49**, 1067–1079.
57 P. M. Oliver, J. A. Crooks, M. Leidl, E. J. Yoon, A. Saghatelian and D. B. Weibel, Localization of anionic phospholipids in *Escherichia coli* cells, *J. Bacteriol.*, 2014, **196**, 3386–3398.
58 N. Noinaj, A. J. Kuszak, C. Balusek, J. C. Gumbart and S. K. Buchanan, Lateral opening and exit pore formation are required for BamA function, *Structure*, 2014, **22**, 1055–1062.
59 R. Wu, J. W. Bakelar, K. Lundquist, Z. Zhang, K. M. Kuo, D. Ryoo, Y. T. Pang, C. Sun, T. White, T. Klose, W. Jiang, J. C. Gumbart and N. Noinaj, Plasticity within the barrel domain of BamA mediates a hybrid-barrel mechanism by BAM, *Nat. Commun.*, 2021, **12**, 7131.
60 J. Thoma, Y. Sun, N. Ritzmann and D. J. Muller, POTRA Domains, Extracellular Lid, and Membrane Composition Modulate the Conformational Stability of the beta Barrel Assembly Factor BamA, *Structure*, 2018, **26**, 987–996.
61 P. J. Fleming, D. S. Patel, E. L. Wu, Y. Qi, M. S. Yeom, M. C. Sousa, K. G. Fleming and W. Im, BamA POTRA Domain Interacts with a Native Lipid Membrane Surface, *Biophys. J.*, 2016, **110**, 2698–2709.
62 N. Csoma, J. M. Machin, J. M. Whitehouse, R. Rodriguez-Alonso, M. Olejnik, A. K. Cahill, S. H. Cho, T. F. Schaberle, B. I. Iorga, N. A. Ranson, S. E. Radford, A. N. Calabrese and J. F. Collet, Molecular insights into how the motions of the beta-barrel and POTRA domains of BamA are coupled for efficient function, *Nat. Commun.*, 2025, **16**, 8832.
63 C. Tanford, Protein denaturation. C. Theoretical models for the mechanism of denaturation, *Adv. Protein Chem.*, 1970, **24**, 1–95.
64 G. H. Huysmans, S. A. Baldwin, D. J. Brockwell and S. E. Radford, The transition state for folding of an outer membrane protein, *Proc. Natl. Acad. Sci. U. S. A.*, 2010, **107**, 4099–4104.
65 H. Hong, S. Park, R. H. Jimenez, D. Rinehart and L. K. Tamm, Role of aromatic side chains in the folding and thermodynamic stability of integral membrane proteins, *J. Am. Chem. Soc.*, 2007, **129**, 8320–8327.
66 T. J. Knowles, D. F. Browning, M. Jeeves, R. Maderbocus, S. Rajesh, P. Sridhar, E. Manoli, D. Emery, U. Sommer, A. Spencer, D. L. Leyton, D. Squire, R. R. Chaudhuri, M. R. Viant, A. F. Cunningham, I. R. Henderson and M. Overduin, Structure and function of BamE within the outer membrane and the beta-barrel assembly machine, *EMBO Rep.*, 2011, **12**, 123–128.
67 G. Mamou, F. Corona, R. Cohen-Khait, N. G. Housden, V. Yeung, D. Sun, P. Sridhar, M. Pazos, T. J. Knowles, C. Kleanthous and W. Vollmer, Peptidoglycan maturation controls outer membrane protein assembly, *Nature*, 2022, **606**, 953–959.
68 H. Takeda, J. V. Busto, C. Lindau, A. Tsutsumi, K. Tomii, K. Imai, Y. Yamamori, T. Hirokawa, C. Motono, I. Ganesan, L. S. Wenz, T. Becker, M. Kikkawa, N. Pfanner, N. Wiedemann and T. Endo, A multipoint guidance mechanism for beta-barrel folding on the SAM complex, *Nat. Struct. Mol. Biol.*, 2023, **30**, 176–187.
69 S. Herwig and J. H. Kleinschmidt, The Formation of beta-Strand Nine (beta(9)) in the Folding and Insertion of BamA from an Unfolded Form into Lipid Bilayers, *Membranes*, 2023, **13**, 247.
70 D. Ni, Y. Wang, X. Yang, H. Zhou, X. Hou, B. Cao, Z. Lu, X. Zhao, K. Yang and Y. Huang, Structural and functional analysis of the beta-barrel domain of BamA from *Escherichia coli*, *FASEB J.*, 2014, **28**, 2677–2685.
71 D. F. Browning, S. A. Matthews, A. E. Rossiter, Y. R. Sevastsyanovich, M. Jeeves, J. L. Mason, T. J. Wells, C. A. Wardius, T. J. Knowles, A. F. Cunningham, V. N. Bavro, M. Overduin and I. R. Henderson, Mutational and topological analysis of the *Escherichia coli* BamA protein, *PLoS One*, 2013, **8**, e84512.
72 Z. C. Ruhe, A. B. Wallace, D. A. Low and C. S. Hayes, Receptor polymorphism restricts contact-dependent growth inhibition to members of the same species, *mBio*, 2013, **4**, e00480–00413.
73 K. M. Storek, M. R. Auerbach, H. Shi, N. K. Garcia, D. Sun, N. N. Nickerson, R. Vij, Z. Lin, N. Chiang, K. Schneider, A. T. Wecksler, E. Skippington, G. Nakamura, D. Seshasayee, J. T. Koerber, J. Payandeh, P. A. Smith and S. T. Rutherford, Monoclonal antibody targeting the beta-barrel assembly machine of *Escherichia coli* is bactericidal, *Proc. Natl. Acad. Sci. U. S. A.*, 2018, **115**, 3692–3697.
74 J. Lee, M. Xue, J. S. Wzorek, T. Wu, M. Grabowicz, L. S. Gronenberg, H. A. Sutterlin, R. M. Davis, N. Ruiz, T. J. Silhavy and D. E. Kahne, Characterization of a stalled

complex on the beta-barrel assembly machine, *Proc. Natl. Acad. Sci. U. S. A.*, 2016, **113**, 8717–8722.

75 C. L. Hagan, J. S. Wzorek and D. Kahne, Inhibition of the beta-barrel assembly machine by a peptide that binds BamD, *Proc. Natl. Acad. Sci. U. S. A.*, 2015, **112**, 2011–2016.

76 J. Lee, D. Tomasek, T. M. Santos, M. D. May, I. Meuskens and D. Kahne, Formation of a beta-barrel membrane protein is catalyzed by the interior surface of the assembly machine protein BamA, *Elife*, 2019, **8**, e49787.

77 H. de Cock, K. Brandenburg, A. Wiese, O. Holst and U. Seydel, Non-lamellar structure and negative charges of lipopolysaccharides required for efficient folding of outer membrane protein PhoE of *Escherichia coli*, *J. Biol. Chem.*, 1999, **274**, 5114–5119.

78 E. M. Germany, N. Thewasano, K. Imai, Y. Maruno, R. S. Bamert, C. J. Stubenrauch, R. A. Dunstan, Y. Ding, Y. Nakajima, X. Lai, C. T. Webb, K. Hidaka, K. S. Tan, H. Shen, T. Lithgow and T. Shiota, Dual recognition of multiple signals in bacterial outer membrane proteins enhances assembly and maintains membrane integrity, *Elife*, 2024, **12**, RP90274.

79 B. Schiffrin, D. J. Brockwell and S. E. Radford, Outer membrane protein folding from an energy landscape perspective, *BMC Biol.*, 2017, **15**, 123.